Discovery of isoliquiritigenin analogues that reverse acute hepatitis by inhibiting macrophage polarization

Junjie Yang [a],[1], Fanjie Hu [a],[1], Chengjun Guo [b],[1], Yuqing Liang [a], Haiying Song [a], Kui Cheng [a],[*]

[a] Guangdong Provincial Key Laboratory of New Drug Screening and Guangzhou Key Laboratory of Drug Research for Emerging Virus Prevention and Treatment, School of Pharmaceutical Sciences, Southern Medical University, Guangzhou 510515, China
[b] School of Applied Mathematics, Guangdong University of Technology, 510006, China

ARTICLE INFO

ABSTRACT

Screening a natural product library of 850 compounds yield isoliquiritigenin as an effective anti-inflammatory agent by inhibiting the production of pro-inflammatory NO induced by Pam_3CSK_4, while its activity accompanied by toxicity. Further studies obtained the optimized isoliquiritigenin derivative $SMU-B_{14}$, which can inhibit Pam_3CSK_4 triggered toll-like receptor 2 (TLR2) signaling with low toxicity and high potency. Preliminary mechanism studies indicated that $SMU-B_{14}$ worked through TLR2/MyD88, phosphorylation of IKKα/β, leading to the reduce degradation of NF-κB related IKBα and p65 complex, then inhibited the production of inflammatory cytokines, such as TNF-α, IL-6, IL-1β both in human and murine cell lines. Subsequent polarization experiments showed $SMU-B_{14}$ significant reversed the polarization of M1 phenotype primary macrophage activated by Pam_3CSK_4 *in vitro*, and reduced the infiltration of neutrophil and polarization of M1-type macrophage, decreased serum alanine transaminase (ALT), as a result protected liver from being injured *in vivo*. In summary, we obtained an optimized lead compound $SMU-B_{14}$ and found it functionally blocked TLR2/MyD88/NF-κB signaling pathway to down-regulate the production of inflammatory cytokines resulted significant liver protection property.

1. Introduction

In the initiation of innate immune responses against pathogen-associated molecule patterns (PAMPs) and damaged-associated molecular patterns (DAMPs), pattern recognition receptors (PRR) were of great importance in recognizing specific components of antigen and triggering immune responses to regulate the balance of host's internal environment[1–2]. Toll-like receptors (TLRs) were discovered earliest and well-studied in family of PRRs. To date, ten subtypes of TLRs have been found in human and distinguished based on their cellular localization: TLR1, 2, 5, 6 and 10 are extracellular receptors, while TLR3, 7, 8 and 9 are intracellular receptors [3,4]. Apart from TLR3, other TLRs recruited the adapter, myeloid differentiation primary response gene 88 (MyD88) to Toll/IL-1 receptor resistance (TIR) domains, resulting in downstream signaling culminating in pro-inflammatory cytokine production[5]. Drug developments based on TLRs had achieved great success. In 1997, TLR7 agonist Imiquimod was approved by FDA for the treatment of condyloma acuminatum, superficial basal cell carcinoma,

and actinic keratosis. The TLR4 agonist MPLA has been used as an FDA-approved adjuvant for cervical cancer vaccines. In addition, TLR2 has attracted more attention for its potent pre-clinical research value[6–12]. Once TLR2 combined with its ligand Pam_3CSK_4, MyD88 were recruited to initiate downstream pathways, resulting in the activation of NF-κB and MAPK signaling pathway. As a result, pro-inflammatory cytokines were released and conducted inflammatory response, such as TNF-α, IL-6, IL-1β[11]. Thus, targeting TLR2 would be a potential target for inflammatory therapy. Rangasamy *et al* found that selective disruption of TLR2 inhibited inflammation and attenuates Alzheimer's pathology [13]. Lyme Arthritis also been reported associate with activation of TLR2 in T cells[14]. In invasive Candida albicans infection, inhibition of TLR2 can reduce the inflammatory response during infection [15]. In recent years, there were certain inhibitors of TLR2 had been found (Fig. 1)[16–22]. However, most of them had moderate TLR2 inhibitory activity or unstable structure, which limited their subsequent researches.

According to the Global Burden of Disease project, >2 million people

---

dead for liver disease including hepatitis, cirrhosis, and liver cancer each year, which accounted for approximately 4% of all deaths worldwide [23]. Clinical research indicated that the process of cirrhosis and liver cancer was closely related to hepatitis[24]. Therefore, the treatment of hepatitis was particularly important in preventing the deterioration of liver disease. The over-activation of TLR2 played a role in the progress of hepatitis, which have been reported by researchers[25–27]. In mouse fatal hepatitis, extracellular histones activated TLR2 to up-regulate the release of inflammatory cytokines[26]. Blockage of TLR2 also delayed liver fibrosis and steatosis caused by hepatitis via regulating NF-κB and MAPK signaling pathways[27]. Hence, TLR2 could be a potential therapeutic target for hepatitis.

The therapeutic properties of plants had been a concern since ancient time. Many researchers focused on natural products so as to discover candidate for hepatitis therapy. For example, Silymarin, extracted from *Silybum marianum*, suppressed liver injury caused by Acetaminophen overdose significantly[28]. Oleanolic acid, found in many medicinal herbs, showed liver-protective effects in LPS/D-GalN-induced fulminant hepatic failure mice[29]. Natural products have been an important source of drug discovery. It was a thrilling news that there were 9 natural products among 38 chemicals which were approved by FDA in 2019 [30].

Herein, through a cell-based screening of 850 natural products, it was found that isoliquiritin was an effective anti-inflammatory agent by using Pam_3CSK_4 (TLR2 agonist) induced nitric oxide (NO) as a reporter indicator. In order to improve its TLR2 inhibitory activity and reduce its toxicity, studies of structure–activity relationship (SAR) were carried out. An optimized isoliquiritigenin derivative SMU-B_{14} was obtained and found it could inhibit the production of pro-inflammatory NO induced by Pam_3CSK_4 in primary mouse peritoneal macrophage with IC_{50} of $1.55 \pm 0.12\,\mu M$ with lower toxicity compared to isoliquiritigenin. Preliminary investigation indicated that SMU-B_{14} reduced the release of inflammatory cytokines in human and murine cell lines, such as TNF-α, IL-6, IL-1β. The macrophage polarization experiment revealed that SMU-B_{14} reduced M1 phenotype macrophage significantly at 10 μM. Further studies indicated that SMU-B_{14} down-regulated the expression of TLR2, suppressed the recruitment of adapter MyD88, and impaired the phosphorylation of NF-κB-p65, leading to an anti-inflammatory effect. Subsequent *in vivo* experiment identified that SMU-B_{14} protected liver from being injured in mice acute hepatitis model by reducing the infiltration

of neutrophile and pro-inflammatory macrophage. In short, we obtained SMU-B_{14} by optimization of isoliquiritigenin which was found as an anti-inflammatory agent by a cell-based screening of 850 natural product compounds, and elucidated its mechanism through TLR2/MyD88/NF-κB signaling pathway showing high anti-inflammatory potency *in vitro* and reverse acute hepatitis *in vivo*.

2. Results

2.1. Screening of potential anti-inflammatory agent and SAR studies.

By screening of 850 nature product compounds from TargetMol L6000, we found isoliquiritigenin (SMU-B_1) could inhibit the release of pro-inflammatory nitric oxide (NO) which triggered by TLR2 agonist Pam_3CSK_4 in mice peritoneal macrophage, but its activity and toxicity coexist. Isoliquiritigenin was isolated from the roots of plants, including *Glycyrrhiza uralensis*, *Mongolian glycyrrhiza*, *Glycyrrhiza glabra*[31]. Based on practical application of *Glycyrrhiza*, pharmacology studies of isoliquiritigenin revealed that it displayed numerous pharmacological properties such as cardioprotective effect[31], anti-cancer[32], anti-diabetes[33], anti-oxidative[34] and so on, but embryotoxicity was observed in zebrafish[35]. Given that, we synthesized a series of derivatives of SMU-B_1 in order to obtain a lead compound with optimized activity and lower toxicity. The structure–activity relationship (SAR) study route was illustrated in Fig. 2A according the scaffold of isoliquiritigenin.

First, based on the left part of chemical structure (blue color), we planned to investigate whether the hydroxyl was conjugated with carbonyl were essential for its activity and whether its activity would be better when the non-conjugated phenolic hydroxyl group was replaced by electron withdrawing group as well as benzene substitution. Second, as for the middle part (pink color), we wanted to find out whether the carbonyl conjugated to alkenyl was necessary for its activity, so we synthesized cyclic derivatives. The third part (red color), we increased the number of electronic donating group, replaced the hydroxyl with electronic-withdrawing group and displayed naphthalene instead of benzene to investigate the electronic and steric effects. As shown in Table 1 **and** Table 2, from compound 1–5 and 14, we knew that the R1 position covered by a hydroxyl group to conjugate with carbonyl group was beneficial to its activity. As for the position of R2, the electron-
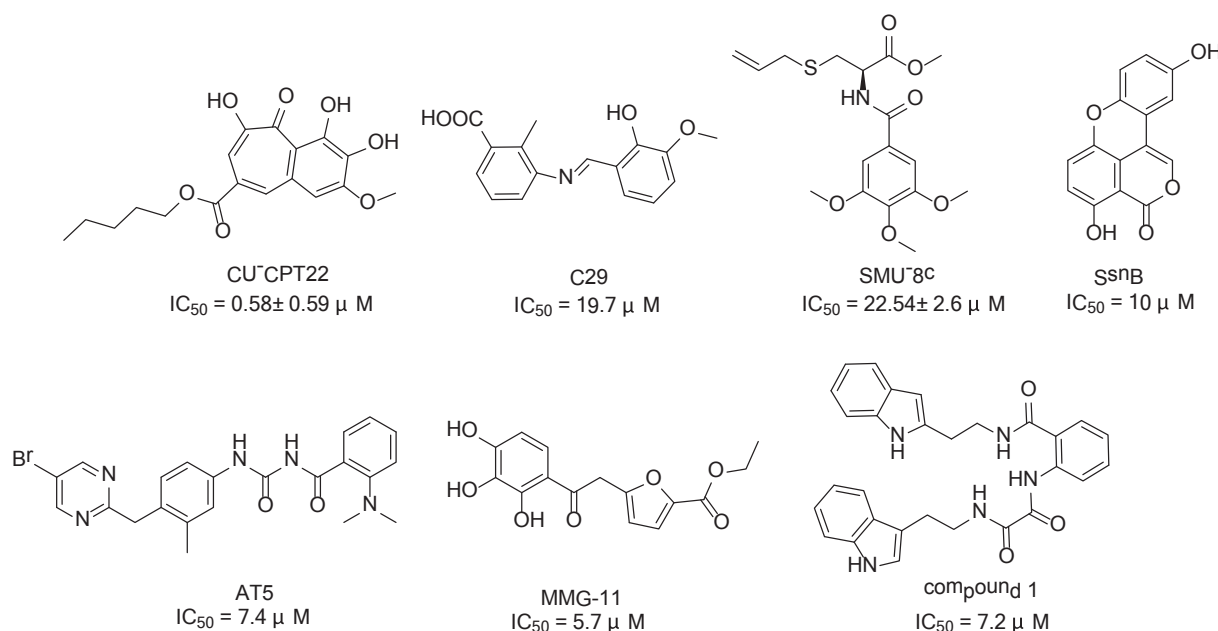

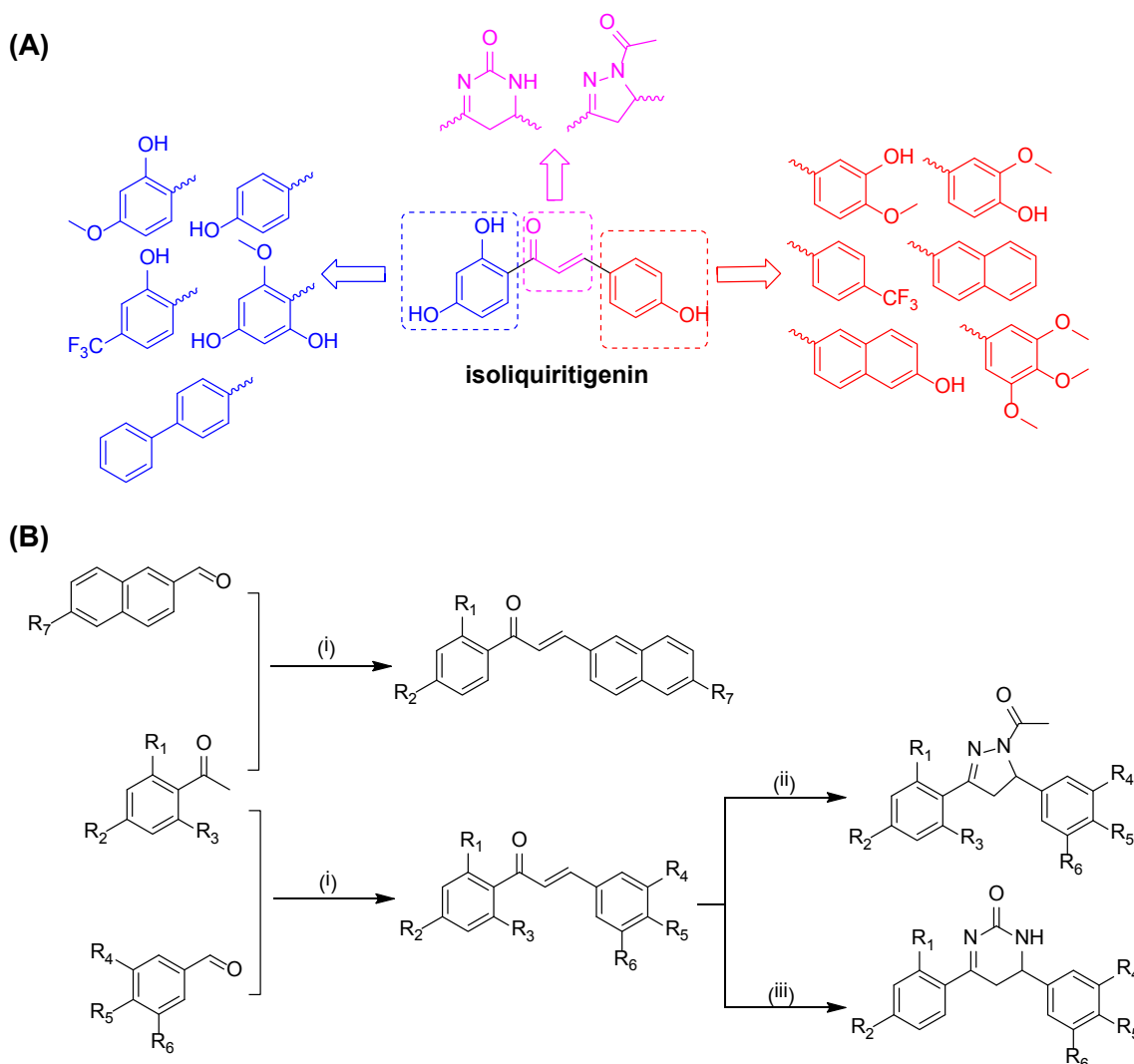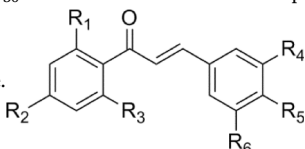**Fig. 1.** The structures and IC_{50} of the reported TLR2 inhibitors.

Fig. 2. The design and synthesis of isoliquiritigenin derivatives. (A) Design of isoliquiritigenin derivatives. (B) Synthesis route of isoliquiritigenin and its derivatives. Reagents and conditions: (i) $SOCl_2$, EtOH, 0 °C to rt, 4 h. (ii) $N_2H_4 \cdot H_2O$, AcOH, rf, 12 h. (iii) $CO(NH_2)_2$, EtOH, Hydrochloric acid 1,4-dioxane, rt, 12 h.

donating group (such as methoxy or hydroxyl) still maintains its activity, but the electron withdrawing or aromatic nucleus weakens its activity, which can be derived from compounds 2, 4, 5, and 12–16. As shown in Table 3, according to compounds 24–40, we can realize that the carbonyl group conjugated with the alkenyl group is necessary for its activity. For the third part, both substituted naphthalene and substituted benzene exhibit similar activity (Table 2). The addition of electron donor groups has little effect on its activity, while electronic-withdrawing group, trifluoromethyl, impaired its activity (Table 1).
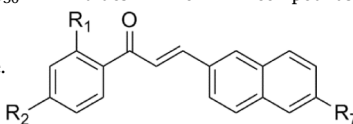
Fortunately, after SAR research, the SMU-B_{14} we obtained not only showed optimized activity to reduce the production of NO in primary mouse peritoneal macrophages with IC_{50} of $1.55 \pm 0.12 \mu M$, but also has lower toxicity compared with isoliquiritigenin (Fig. 3A-B). Given that TLR2 can dimer with either TLR1 or TLR6, we wonder to know how SMU-B_{14} affects TLR1/2 and TLR2/6. As shown in Fig. 3A, SMU-B_{14} was a complete TLR2 inhibitor, suppressing the NO signaling induced by TLR1/2 and TLR2/6 ligands. In short, we obtained an isoliquiritigenin derivative SMU-B_{14} which performed potent activity against TLR2 and displayed less toxicity compared to isoliquiritigenin (Fig. 3).

2.2. SMU-B_{14} reduced the production of inflammatory cytokines and polarization of macrophage into M1 phenotype

Isoliquiritigenin with a wide range of physiological activities has been reported to inhibit the inflammation caused by TLR4[36], but the relationship between isoliquiritigenin and TLR2 has not been reported by others. For it was observed that the isoliquiritigenin analogue SMU-B_{14} inhibited the release of pro-inflammatory NO induced by Pam_3CSK_4, we hypothesized that SMU-B_{14} blocked TLR2 and its downstream signaling pathways, thereby reducing the release of inflammatory cytokines. We performed ELISA to detect inflammatory cytokines both in human and murine cell lines. As illustrated in Fig. 4A, after treatment with SMU-B_{14}, Pam_3CSK_4-induced TNF-α secretion in Raw 264.7 cells decreased, and TNF-α as well as IL-6 also showed a dose-dependent decline tendency in peritoneal macrophages with 80% inhibition at the present of 10 μM SMU-B_{14} (Fig. 4B-C). Activation of dendritic cells (DCs) enhanced its antigen presentation ability, acting as a bridge between innate and adaptive immune. In mouse bone marrow-derived dendritic cells (BMDCs), we found SMU-B_{14} reduced the 80% production of IL-6 at 5 μM (Fig. 4D). In human cell lines, as we expected, SMU-B_{14} played an effect on eliminating the production of TNF- α in PMA differential human myeloid leukemia mononuclear cells (THP-1 cells) (Fig. 4E). Similar results also observed in the *ex-vivo* human peripheral

Table 1

The IC_{50} values of compounds in peritoneal macrophage.

Compound	R1	R2	*R3*	R4	R5	R6	IC_{50} (μM)
1	OH	OH	H	H	OH	H	2.5 ± 0.15
2	OH	OH	H	OCH$_3$	OH	H	2.8 ± 0.17
3	H	OH	H	OH	OCH$_3$	H	4.62 ± 0.53
4	H	OH	H	OCH$_3$	OH	H	3.71 ± 0.27
5	H	OH	H	H	OH	H	4.8 ± 0.36
6	H	OH	H	H	CF$_3$	H	12.97 ± 2.77
7	H	OH	H	OCH$_3$	OCH$_3$	OCH$_3$	1.77 ± 0.12
8	OH	OCH$_3$	H	H	OH	H	7.73 ± 0.34
9	OH	OCH$_3$	H	OH	OCH$_3$	H	2.78 ± 0.07
10	OH	OCH$_3$	H	OCH$_3$	OH	H	2.89 ± 0.28
11	OH	OCH$_3$	H	H	CF$_3$	H	>50
12	OH	CF$_3$	H	OCH$_3$	OH	H	>50
13	OH	CF$_3$	H	OH	OCH$_3$	H	6.67 ± 1.38
14 (SMU-B$_{14}$)	OH	OH	H	OH	OCH$_3$	H	1.55 ± 0.12
15	H	Bn	H	H	OH	H	5.37 ± 0.54
16	H	Bn	H	OCH$_3$	OH	H	>50
17	OH	OH	OCH$_3$	H	H	H	1.88 ± 0.08

Table 2

The IC_{50} values of compounds in peritoneal macrophage.

Compound	R1	R2	R7	IC_{50} (μM)
18	OH	OH	OH	4.27 ± 1
19	H	OH	H	1.67 ± 0.29
20	OH	OCH$_3$	H	1.65 ± 0.27
21	OH	OCH$_3$	OH	1.68 ± 0.32
22	H	Bn	H	>50
23	H	Bn	OH	>50

blood mononuclear cells (PBMCs). SMU-B$_{14}$ performed better at preventing the production of IL-1β than TNF-α, inhibiting nearly 90% at 2.5 μM (Fig. 4F-G). In addition, inflammatory cytokines induced by TLR2/6 agonist Pam$_2$CSK$_4$, such as TNF-α, IL-6, IL-1β, were both declined in human and murine cell lines, which also suggested that SMU-B14 was a totally TLR2 inhibitor (Fig. 4H-J).

The pro-inflammatory NO was mainly produced by inducible nitric oxide synthase (iNOS), which was highly expressed in macrophage after stimulation of TLR ligands[36]. Such highly expressed iNOS macrophage promoted inflammatory response and was defined as M1 phenotype macrophage[37]. In peritoneal macrophage, we analyzed the polarization of M1 phenotype macrophage by detecting the specific marker CD86 with flow cytometry. As shown in Fig. 4K, Pam$_3$CSK$_4$ promoted the polarization of macrophages into M1 phenotype with an increased expression of CD86. It is worth noting that SMU-B$_{14}$ significantly reduced the expression of CD86 at 10 μM, indicating that the polarization of the M1 phenotype was hindered. From above experiments, we can conclude that SMU-B$_{14}$ reduces the release of inflammatory cytokines induced by TLR2 agonist both in human and murine cell lines, and impairs inflammation by reducing the inflammatory macrophage M1 phenotype. However, its anti-inflammatory mechanisms remains not clear.

2.3. SMU-B$_{14}$ blocked the activation of TLR2/MyD88/NF-κB signaling pathway

We next to investigate whether SMU-B$_{14}$ targeted TLR2 and its downstream signaling pathway to perform its anti-inflammatory effect. To verify SMU-B$_{14}$ had an effect on TLR2, we conducted Western Blot assay in THP-1 (human cell line) and Raw 264.7 (murine cell line) cells. The expression of TLR2 was up-regulated after treatment with Pam$_3$CSK$_4$ both in THP-1 and Raw 264.7 cells, which can be reversed by SMU-B$_{14}$ (Fig. 5A-B). TLR2 adapter protein MyD88 was investigated in THP-1 cell for we hadn't observed significant up-regulation in Raw 264.7 cells after Pam$_3$CSK$_4$ treatment. SMU-Z1, a reported TLR1/2 agonist, was used instead of Pam$_3$CSK$_4$. As shown in Fig. 5C, the recruitment of MyD88 mediated by TLR2 agonist decreased under the treatment of SMU-B$_{14}$. According to previous studies, TLR2 recruited MyD88 to activate NF-κB and MAPK pathways[17]. As shown in Fig. 5D, upon SMU-B$_{14}$ treatment, phosphorylated p65 and phosphorylated IKKα/β were down-regulated at 15 and 30 min. After Pam$_3$CSK$_4$ treatment for 30 min, IKBα was significantly degraded, which can be prevented by SMU-B$_{14}$. Meanwhile, SMU-B$_{14}$ seen to have an inhibition on phosphorylated p38 related to MAPK pathway but not as robust as NF-κB pathway (Fig. 5D), indicating that SMU-B$_{14}$ displayed a certain selectivity in inhibition of NF-κB signaling pathway. In general, we identified SMU-B$_{14}$ mainly worked by inhibiting TLR2/MyD88/NF-κB pathway to play an anti-inflammatory effect.

2.4. SMU-B$_{14}$ reduced liver injury caused by acute hepatitis
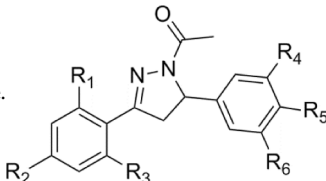
TLR2 played an effect on the process of hepatitis, which had been reported in previous studies[25–27]. We wondered whether TLR2 could serve as therapeutic target for hepatitis. It had been reported that Myd88$^{-/-}$ mice suffered from less liver injury when intravenously administered with Concanavalin A[38]. Therefore, we established mice model of acute hepatitis by intravenously administered with Concanavalin A to investigate whether SMU-B$_{14}$ could reduce liver injury. Compared with control, Concanavalin A can cause acute hepatitis in the model mice after 6 h of stimulation, and the addition of SMU-B$_{14}$ at the specified concentration can significantly reverse liver damage (Fig. 6A). The histological section of the liver showed that the infiltration of liver neutrophils was significantly reduced after SMU-B$_{14}$ treatment (Fig. 6B). We also evaluated the polarization of macrophages by detecting the expression of iNOS[39]. As shown in Fig. 6C, immunohistochemical results of iNOS showed that the expression of iNOS in the liver of mice increased significantly after Concanavalin A treatment. This result indicated that the infiltration of M1 phenotypic macrophages in the liver was increased, and more pro-inflammatory NO was secreted into the liver tissue. In contrast, after SMU-B$_{14}$ treatment, the expression of iNOS in liver decreased significantly. Reduced infiltration of neutrophils and reduced inflammatory macrophages alleviated the liver damage caused by acute hepatitis, which could be validated by the detection of lower serum ALT after SMU-B$_{14}$ treatment (Fig. 6D). In short, SMU-B$_{14}$ could reduce the accumulation of neutrophils and the polarization of M1 phenotype macrophages, thereby reducing acute hepatitis damage and improving liver function.
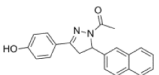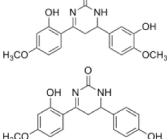
3. Discussion

Liver disease accounts for approximately 2 million deaths per year worldwide and most of them suffered from hepatitis in different degree [23]. Inhibition of TLR2 has been identified to alleviat hepatitis[25–27]. In this study, we found isoliquiritigenin as an anti-inflammatory agent by a cell based scanning of 850 natural products (Fig. 7). Although it displayed inhibitory activity against pro-inflammatory NO induced by TLR2 in primary peritoneal macrophage, its activity accompanied by toxicity. In order to improve its anti-inflammatory activity and reduce toxicity, SAR studies were carried out and SMU-B$_{14}$ performed

Table 3

The IC$_{50}$ values of compounds in peritoneal macrophage.

Compound	R1	R2	R3	R4	R5	R6	IC$_{50}$ (μM)
24	OH	OH	H	H	OH	H	>50
25	OH	OH	H	OCH$_3$	OH	H	>50
26	OH	OH	H	OH	OCH$_3$	H	>50
27	H	OH	H	H	OH	H	>50
28	H	OH	H	H	OH	OCH$_3$	>50
29	H	OH	H	H	OCH$_3$	OH	>50
30	H	OH	H	H	CF$_3$	H	>50
31	OH	OCH$_3$	H	H	OH	H	>50
32	OH	OCH$_3$	H	OH	OCH$_3$	H	>50
33	OH	OCH$_3$	H	OCH$_3$	OH	H	>50
34	OH	OCH$_3$	H	OCH$_3$	OCH$_3$	OCH$_3$	>50
35	H	Bn	H	OCH$_3$	OH	H	8.99 ± 1.93
36	OH	OH	OCH$_3$	H	H	H	>50
37	OH	CF$_3$	H	OCH$_3$	OH	H	>50
38							>50
39							8.08 ± 1.92
40							>50

optimized anti-inflammatory effect and less toxicity compared to iso-liquiritigenin. Preliminary anti-inflammatory mechanism studies indicated SMU-B$_{14}$ inhibited the production of inflammatory factors induced by Pam$_3$CSK$_4$ in human and murine cell lines (Fig. 4A-G). Subsequent polarization experiments showed SMU-B$_{14}$ significantly reversed the polarization of M1 phenotype primary peritoneal macrophage activated by Pam$_3$CSK$_4$ *in vitro*, which accounted for NO signaling inhibition in primary peritoneal macrophage. Further mechanism investigation suggested that SMU-B$_{14}$ worked through TLR2/MyD88/NF-κB signaling pathway to down-regulate the release of inflammatory cytokines (Fig. 7). Although Pam$_3$CSK$_4$ activated both NF-κB and MAPK signaling pathway, SMU-B$_{14}$ prefered to block the former. Next, We established a mice model of acute hepatitis to investigat whether SMU-B$_{14}$ could alleviate hepatitis. As expected, SMU-B$_{14}$ reduced the inflammation in liver induced by Concanavalin A. Further liver histological sections showed that less neutrophil infiltration in liver was observed after adminstration of indicated SMU-B$_{14}$ (Fig. 6B). Meanwhile, immunohistochemistry results suggested that SMU-B$_{14}$ reduced the the polarization of M1 phenotype macrophage in liver since less M1 phenotype macrophage marker iNOS was detected (Fig. 6C). As a result, liver function was improved, which could be validated by lower seurm ALT detected after SMU-B$_{14}$ treatment. In summary, we conducted SAR research on isoliquiritigenin and found an optimized anti-inflammatory agent SMU-B$_{14}$ with low toxicity and high potency, revealing its mechanism by blocking TLR2/MyD88/NF-κB signaling pathway to reduce the production of inflammatory cytokines *in vitro* and validated its anti-inflammatory and liver-protective effect in acute hepatitis *in vivo*.

4. Experimental section

4.1. Chemistry

General procedure for synthesis of compound **1–24**

Compound 1–24 were synthesized as follow: the mix of acetophenone analogues (1 mmol) and benzaldehyde analogues (1.1 mmol) in ethanol (10 mL) was cooled at 0 °C. Thionyl chloride (5 mmol) was added in slowly. After the thionyl chloride was added in, the whole mixture was kept in room temperature and reacted for 4 h. After completion of the reaction, the ethanol was removed under vacuum. The residues were dissolved in Ethyl acetate (20 mL) and deionized water (10 mL) was added in for extraction. The organic phase was kept and washed by saturated sodium bicarbonate aqueous solution (10 mL), saturated saline (10 mL). The solvent was evaporated to dryness under reduced pressure. The crude product was purified by flash column chromatography on silica gel (petroleum ether/ethyl acetate elute) to provide the compound **1–23**.

(E)-1-(2,4-dihydroxyphenyl)-3-(4-hydroxyphenyl)prop-2-en-1-one (compound **1**)

Yellow solid, yield: 74%. ^{1}H NMR (400 MHz, DMSO-d_6) δ 13.60 (s, 1H), 10.66 (s, 1H), 10.14 (s, 1H), 8.16 (d, J = 8.8 Hz, 1H), 7.75 (s, 4H), 6.85 (d, J = 8.1 Hz, 2H), 6.41 (d, J = 8.8 Hz, 1H), 6.29 (s, 1H).^{13}C NMR (101 MHz, DMSO-d_6) δ 191.92, 166.17, 165.33, 160.65, 144.66, 133.24, 131.61, 126.15, 117.81, 116.24, 113.40, 108.49, 102.98 . ESI-MS: m/z calcd for C$_{15}$H$_{12}$NaO$_4$ (M + Na$^+$) 279.0, found 279.0.

(E)-1-(2,4-dihydroxyphenyl)-3-(4-hydroxy-3-methoxyphenyl)prop-2-en-1-one (compound **2**)

Yellow solid, yield: 69%. ^{1}H NMR (400 MHz, DMSO-d_6) δ 13.54 (s, 1H), 10.69 (s, 1H), 9.14 (s, 1H), 8.17 (d, J = 8.9 Hz, 1H), 7.76 – 7.66 (m, 2H), 7.36 – 7.29 (m, 2H), 7.01 (d, J = 8.3 Hz, 1H), 6.41 (d, J = 8.9 Hz, 1H), 6.28 (s, 1H), 3.85 (s, 3H).^{13}C NMR (101 MHz, DMSO-d_6) δ 191.84, 166.15, 165.42, 150.81, 147.05, 144.65, 133.34, 127.99, 122.67, 118.85, 115.51, 113.42, 112.31, 108.54, 102.97, 56.12 . ESI-MS: m/z calcd for C$_{16}$H$_{14}$O$_5$ (M + H$^+$) 287.0, found 287.0.

(E)-3-(3-hydroxy-4-methoxyphenyl)-1-(4-hydroxyphenyl)prop-2-en-1-one (compound **3**)

Yellow solid, yield: 69%. ^{1}H NMR (400 MHz, DMSO-d_6) δ 10.38 (s, 1H), 9.15 (s, 1H), 8.16 – 7.89 (m, 2H), 7.72 – 7.49 (m, 2H), 7.36 – 7.17 (m, 2H), 7.04 – 6.81 (m, 3H), 3.85 (s, 3H).^{13}C NMR (101 MHz, DMSO-d_6) δ 187.42, 162.34, 150.42, 147.02, 143.57, 131.38, 129.77, 128.22, 122.14, 119.84, 115.71, 115.13, 112.30, 56.07 . ESI-MS: m/z
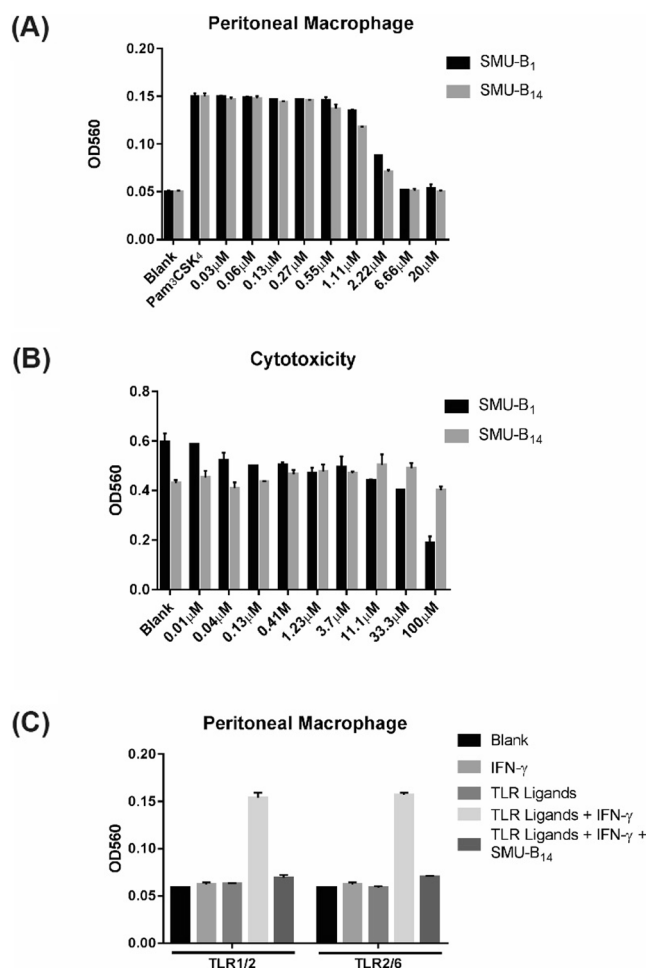
Fig. 3. Comparison between SMU-B₁ and SMU-B₁₄ in inhibition of NO release and cytotoxicity. (A) NO signal of SMU-B₁ and SMU-B₁₄ in mouse peritoneal macrophages. Peritoneal Macrophages were treated with Pam₃CSK₄ 100 ng/mL, interferon -γ 40 ng/mL and indicated SMU-B₁ or SMU-B₁₄ for 24 h. The supernatant was collected for NO test by Griess method. (B) Cytotoxicity for SMU-B₁ and SMU-B₁₄ in mouse peritoneal macrophages were tested by MTT method. (C) Peritoneal Macrophage were treated with Pam₃CSK₄ (or Pam₂CSK₄) 100 ng/mL, interferon-γ 40 ng/mL, Pam₃CSK₄ (or Pam₂CSK₄) 100 ng/mL plus interferon-γ 40 ng/mL, Pam₃CSK₄ (or Pam₂CSK₄) 100 ng/mL plus interferon-γ 40 ng/mL and SMU-B14 20 μM for 24 h. The supernatant was collected for NO test by Griess method. Data presented are mean ± SD and the figures shown are representative of three independent experiments.

calcd for $C_{16}H_{14}O_4$ (M + H$^+$) 271.0, found 271.1.

(E)-3-(4-hydroxy-3-methoxyphenyl)-1-(4-hydroxyphenyl)prop-2-en-1-one (compound **4**)

Yellow solid, yield: 73%. ^{1}H NMR (400 MHz, DMSO-d_6) δ 10.34 (s, 1H), 9.61 (s, 1H), 8.06 (d, J = 8.2 Hz, 2H), 7.76 – 7.59 (m, 2H), 7.49 (s, 1H), 7.25 (d, J = 8.1 Hz, 1H), 6.90 (d, J = 8.2 Hz, 2H), 6.83 (d, J = 8.1 Hz, 1H), 3.88 (s, 3H).^{13}C NMR (101 MHz, DMSO-d_6) δ 187.43, 162.29, 149.78, 148.36, 143.98, 131.37, 129.86, 126.87, 124.21, 119.10, 115.95, 115.67, 111.90, 56.22 . ESI-MS: m/z calcd for $C_{16}H_{14}O_4$ (M + H$^+$) 271.0, found 271.0.

(E)-1,3-bis(4-hydroxyphenyl)prop-2-en-1-one (compound **5**)

Yellow solid, yield: 93%. ^{1}H NMR (400 MHz, DMSO-d_6) δ 10.36 (d, J = 4.5 Hz, 1H), 10.13 – 9.95 (m, 1H), 8.03 (t, J = 10.8 Hz, 2H), 7.67 (dq, J = 29.0, 7.0, 6.3 Hz, 4H), 6.98 – 6.69 (m, 4H). ^{13}C NMR (101 MHz, DMSO-d_6) δ 187.42, 162.28, 160.21, 143.54, 131.33, 131.13, 129.83, 126.38, 118.92, 116.16, 115.68 . ESI-MS: m/z calcd for $C_{15}H_{12}O_3$ (M + H$^+$) 241.0, found 241.0.

(E)-1-(4-hydroxyphenyl)-3-(4-(trifluoromethyl)phenyl)prop-2-en-1-one (compound **6**)

Yellow solid, yield: 73%. ^{1}H NMR (400 MHz, DMSO-d_6) δ 10.47 (s, 1H), 8.13 – 8.02 (m, 5H), 7.80 (d, J = 8.0 Hz, 2H), 7.73 (d, J = 15.6 Hz, 1H), 6.92 (d, J = 8.3 Hz, 2H).^{13}C NMR (101 MHz, DMSO-d_6) δ 187.37, 162.83, 141.09, 139.35, 131.76, 129.64, 129.26, 126.06, 126.02, 125.26, 115.84 . ESI-MS: m/z calcd for $C_{16}H_{11}F_3O_2$ (M + H$^+$) 293.0, found 293.0.

(E)-1-(4-hydroxyphenyl)-3-(3,4,5-trimethoxyphenyl)prop-2-en-1-one (compound **7**)

Yellow solid, yield: 95%. ^{1}H NMR (400 MHz, DMSO-d_6) δ 10.41 (s, 1H), 8.10 (d, J = 8.7 Hz, 2H), 7.87 (d, J = 15.5 Hz, 1H), 7.65 (d, J = 15.5 Hz, 1H), 7.21 (s, 2H), 6.92 (d, J = 8.7 Hz, 2H), 3.87 (s, 6H), 3.72 (s, 3H).^{13}C NMR (101 MHz, DMSO-d_6) δ 187.48, 162.52, 153.50, 143.59, 131.57, 130.85, 129.62, 121.69, 115.73, 106.74, 60.52, 56.52 . ESI-MS: m/z calcd for $C_{18}H_{18}O_5$ (M + H$^+$) 315.1, found 315.1.

(E)-1-(2-hydroxy-4-methoxyphenyl)-3-(4-hydroxyphenyl)prop-2-en-1-one (compound **8**)

Yellow solid, yield: 67%. ^{1}H NMR (400 MHz, DMSO-d_6) δ 13.67 (s, 1H), 10.16 (s, 1H), 8.25 (d, J = 8.9 Hz, 1H), 7.78 (d, J = 11.4 Hz, 4H), 6.86 (d, J = 8.4 Hz, 2H), 6.55 (d, J = 9.0 Hz, 1H), 6.50 (s, 1H), 3.84 (s, 3H).^{13}C NMR (101 MHz, DMSO-d_6) δ 192.28, 166.14, 166.12, 160.80, 145.17, 132.79, 131.75, 126.10, 117.71, 116.26, 114.24, 107.64, 101.32, 56.10 . ESI-MS: m/z calcd for $C_{15}H_{12}O_4$ (M + H$^+$) 256.0, found 256.0.

(E)-1-(2-hydroxy-4-methoxyphenyl)-3-(3-hydroxy-4-methoxyphenyl)prop-2-en-1-one (compound **9**)

Yellow solid, yield: 80%. ^{1}H NMR (400 MHz, DMSO-d_6) δ 13.70 (s, 1H), 9.76 (s, 1H), 8.29 (d, J = 9.0 Hz, 1H), 7.86 – 7.75 (m, 2H), 7.55 (s, 1H), 7.34 – 7.28 (m, 1H), 6.85 (d, J = 8.1 Hz, 1H), 6.57 (dd, J = 8.9, 2.1 Hz, 1H), 6.52 (d, J = 2.3 Hz, 1H), 3.89 (s, 3H), 3.85 (s, 3H).^{13}C NMR (101 MHz, DMSO-d_6) δ 192.31, 166.19, 150.46, 148.44, 145.65, 132.86, 126.55, 125.10, 117.84, 115.99, 114.21, 112.24, 107.69, 101.28, 56.28, 56.14 . ESI-MS: m/z calcd for $C_{17}H_{16}O_5$ (M + H$^+$) 301.1, found 301.1.

(E)-3-(4-hydroxy-3-methoxyphenyl)-1-(2-hydroxy-4-methoxyphenyl)prop-2-en-1-one (compound **10**)

Yellow solid, yield: 85%. ^{1}H NMR (400 MHz, DMSO-d_6) δ 13.70 (s, 1H), 9.76 (s, 1H), 8.29 (d, J = 9.0 Hz, 1H), 7.84 (d, J = 15.3 Hz, 1H), 7.77 (d, J = 15.3 Hz, 1H), 7.56 (d, J = 1.6 Hz, 1H), 7.31 (dd, J = 8.2, 1.7 Hz, 1H), 6.85 (d, J = 8.1 Hz, 1H), 6.57 (dd, J = 9.0, 2.4 Hz, 1H), 6.52 (d, J = 2.4 Hz, 1H), 3.89 (s, 3H), 3.85 (s, 3H).^{13}C NMR (101 MHz, DMSO-d_6) δ 192.31, 166.18, 150.46, 148.44, 145.66, 132.87, 126.55, 125.10, 117.84, 115.99, 114.21, 112.24, 107.70, 101.29, 56.28, 56.14 . ESI-MS: m/z calcd for $C_{17}H_{16}O_5$ (M + H$^+$) 301.1, found 301.1.

(E)-1-(2-hydroxy-4-methoxyphenyl)-3-(4-(trifluoromethyl)phenyl)prop-2-en-1-one (compound **11**)

Yellow solid, yield: 62%. ^{1}H NMR (400 MHz, DMSO-d_6) δ 12.66 (s, 1H), 7.91 (d, J = 8.9 Hz, 1H), 7.69 (q, J = 8.3 Hz, 4H), 6.57 – 6.46 (m, 2H), 5.66 (s, 1H), 5.33 – 5.19 (m, 1H), 3.83 (s, 3H).^{13}C NMR (101 MHz, DMSO-d_6) δ 202.80, 166.11, 164.61, 150.33, 133.53, 127.12, 125.34, 114.48, 107.63, 101.18, 69.15, 56.10, 47.75, 44.41 . ESI-MS: m/z calcd for $C_{17}H_{13}F_3O_3$ (M + H$^+$) 322.0, found 322.0.

(E)-3-(4-hydroxy-3-methoxyphenyl)-1-(2-hydroxy-4-(trifluoromethyl)phenyl)prop-2-en-1-one (compound **12**)

Yellow solid, yield: 53%. ^{1}H NMR (400 MHz, DMSO-d_6) δ 12.50 – 12.28 (m, 1H), 9.89 (s, 1H), 8.26 (d, J = 8.2 Hz, 1H), 7.87 – 7.64 (m, 2H), 7.52 (s, 1H), 7.31 (d, J = 7.3 Hz, 3H), 6.87 (d, J = 8.1 Hz, 1H), 3.88 (s, 3H).^{13}C NMR (101 MHz, DMSO-d_6) δ 193.26, 160.56, 150.84, 148.44, 147.17, 131.96, 126.29, 125.98, 125.19, 119.61, 116.09, 112.44, 56.23 . ESI-MS: m/z calcd for $C_{17}H_{13}F_3O_4$ (M + H$^+$) 338.0, found 338.0.

(E)-1-(2-hydroxy-4-(trifluoromethyl)phenyl)-3-(3-hydroxy-4-methoxyphenyl)prop-2-en-1-one (compound **13**)

Yellow solid, yield: 61%. ^{1}H NMR (400 MHz, DMSO-d_6) δ 9.43 (s, 1H), 8.30 – 8.20 (m, 2H), 7.81 (d, J = 8.2 Hz, 1H), 7.66 (dd, J = 8.5, 2.1 Hz, 1H), 7.54 (d, J = 2.2 Hz, 1H), 7.13 (d, J = 8.6 Hz, 1H), 6.95 (s, 1H), 3.90 (s, 3H).^{13}C NMR (101 MHz, DMSO-d_6) δ 191.65, 148.43, 146.90,
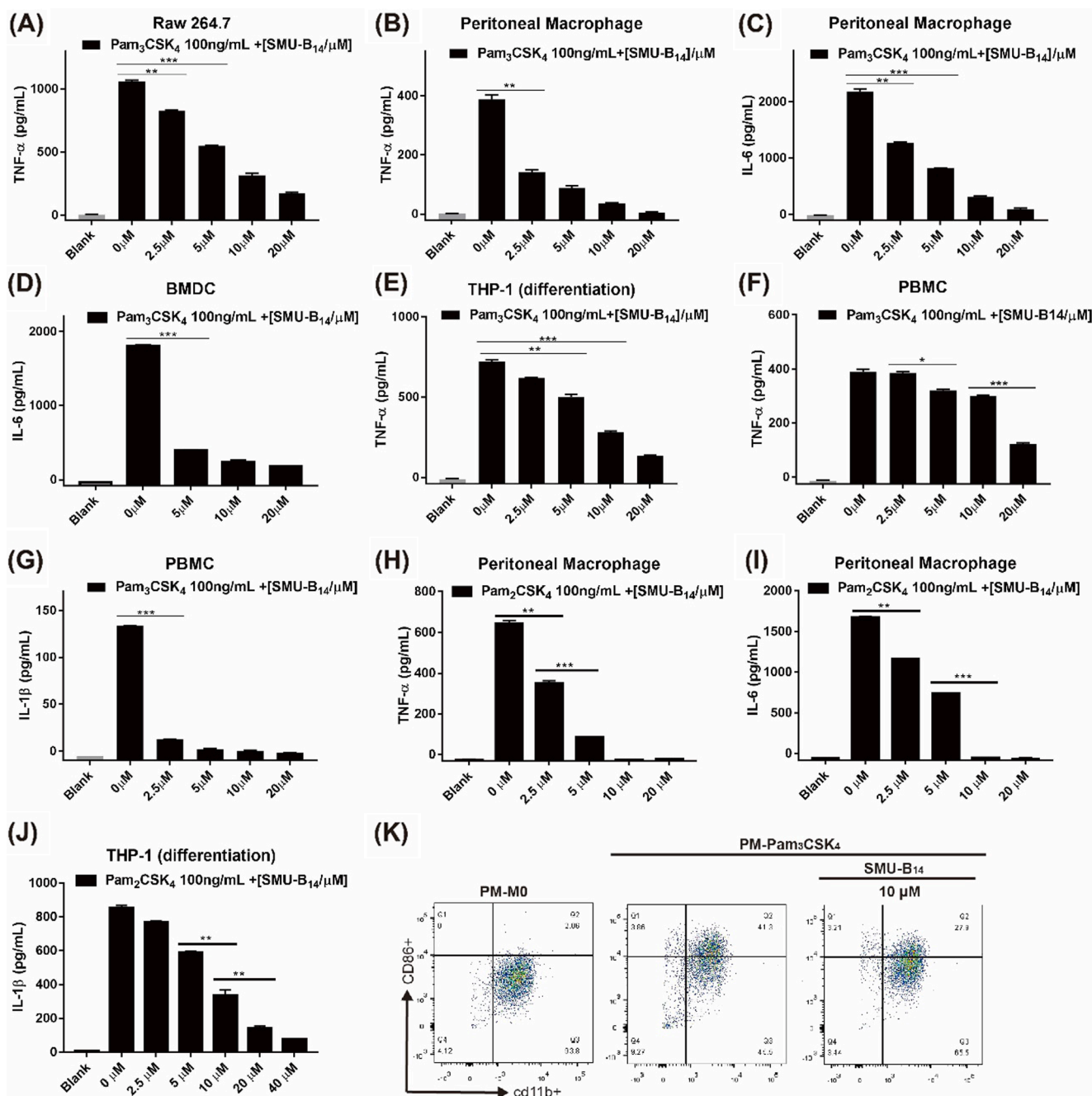
Fig. 4. SMU-B$_{14}$ inhibited the release of TNF-α, IL-6, IL-1β triggered by Pam$_3$CSK$_4$ in human cell lines and murine cell lines. (A) The TNF-α in the supernatants of mouse RAW 264.7 cells after treatment with Pam$_3$CSK$_4$ 100 ng/mL and indicated SMU-B$_{14}$ for 24 h. (B, C) The TNF-α and IL-6 in the supernatants of peritoneal macrophage cells after treatment with Pam$_3$CSK$_4$ 100 ng/mL and indicted SMU-B$_{14}$ for 24 h. (D) The IL-6 signaling in BMDCs were test in the supernatants after treatment with Pam$_3$CSK$_4$ 100 ng/mL and indicated SMU-B$_{14}$ for 24 h. (E) The THP-1 cells were treated with phorbol-12-myristate-13-acetate (PMA) 100 ng/mL for 24 h. The supernatants were removed and the cells were washed with PBS for 3 times. The medium containing Pam$_3$CSK$_4$ 100 ng/mL and indicated SMU-B$_{14}$ were added in and the cells were cultured for 24 h. (F, G) The TNF-a and IL-1β signaling in human primary PBMC cells were test in the supernatants after treatment with Pam$_3$CSK$_4$ 100 ng/mL and indicated SMU-B$_{14}$ for 24 h. (H, I) The TNF-a and IL-6 signaling in murine peritoneal macrophage cells were test in the supernatants after treatment with Pam$_2$CSK$_4$ 100 ng/mL and indicated SMU-B$_{14}$ for 24 h. (J) The IL-1β signaling in THP-1 cells were test in the supernatants after treatment with Pam$_2$CSK$_4$ 100 ng/mL and indicated SMU-B$_{14}$ for 24 h. (K) Flow cytometry analysis of CD86 + and CD11b + in peritoneal macrophage. Cells were treated with medium (PM-M0), IFN-γ (40 ng/mL) plus Pam$_3$CSK$_4$ (100 ng/mL), IFN-γ (40 ng/mL) plus Pam$_3$CSK$_4$ (100 ng/mL) and indicated SMU-B$_{14}$ for 24 h. Data presented are mean ± SD and the figures shown are representative of three independent experiments. (*P ≤ 0.05; **P < 0.01; ***P < 0.001).

132.05, 131.13, 128.24, 123.66, 118.24, 115.88, 115.24, 114.57, 112.39, 79.54, 56.07, 43.51. ESI-MS: *m/z* calcd for C$_{17}$H$_{13}$F$_3$O$_4$ (M + H$^+$) 338.0, found 338.0.

(E)-1-(2,4-dihydroxyphenyl)-3-(3-hydroxy-4-methoxyphenyl)prop-2-en-1-one (compound **14**)

Yellow solid, yield: 72%. ^{1}H NMR (400 MHz, DMSO-d_6) δ 13.65 (s, 1H), 10.70 (s, 1H), 9.75 (s, 1H), 8.21 (d, *J* = 8.8 Hz, 1H), 7.78 (dd, *J* = 13.3, 10.0 Hz, 2H), 7.53 (s, 1H), 7.29 (d, *J* = 7.9 Hz, 1H), 6.84 (d, *J* = 7.8 Hz, 1H), 6.43 (dd, *J* = 8.0, 4.6 Hz, 1H), 6.29 (s, 1H), 3.88 (s, 3H).^{13}C NMR (101 MHz, DMSO-d_6) δ 191.94, 166.22, 165.34, 150.29, 148.43, 145.13, 133.29, 126.62, 124.94, 117.91, 115.98, 113.40, 112.08, 108.45, 103.00, 56.25 . ESI-MS: *m/z* calcd for C$_{16}$H$_{14}$O$_5$ (M + H$^+$) 287.0,
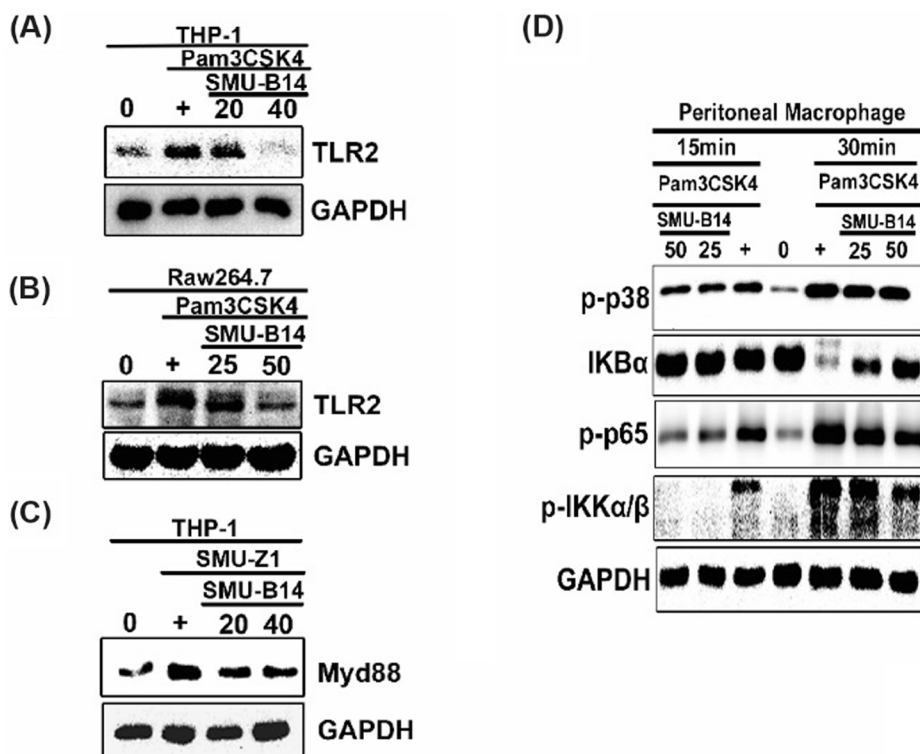
Fig. 5. The inhibit effect of SMU-B$_{14}$ on TLR2, NF-κB pathway and MAPK pathway by Western Blot. (A) THP-1 cells were treated with phorbol-12-myristate-13-acetate (PMA) 100 ng/mL for 24 h. The supernatants were removed and the cells were washed with PBS for 3 times. The medium containing Pam$_3$CSK$_4$ 300 ng/mL and indicated SMU-B$_{14}$ were added in and the cells were cultured for 12 h. (B) Raw264.7 cells were treated with Pam$_3$CSK$_4$ (300 ng/mL) and indicated SMU-B$_{14}$ for 12 h, whole-cell lysates were collected for Western Blot. (C) THP-1 cells were treated with phorbol-12-myristate-13-acetate (PMA) 100 ng/mL for 24 h. The supernatants were removed and the cells were washed with PBS for 3 times. The medium containing SMU-Z1 5 μM/mL and indicated SMU-B$_{14}$ were added in and the cells were cultured for 3 h. (D) Peritoneal macrophage were pre-treated with SMU-B$_{14}$ for 1 h and then treated with Pam$_3$CSK$_4$ (300 ng/mL) for 15 or 30 min. Western Blot was performed using whole-cell lysates and Abs directed against the signaling intermediates indicated.

found 287.1.

(E)-1-([1,1′-biphenyl]-4-yl)-3-(4-hydroxyphenyl)prop-2-en-1-one (compound **15**)

Yellow solid, yield: 63%. ^{1}H NMR (400 MHz, DMSO) δ 9.69 (s, 1H), 8.24 (d, *J* = 8.0 Hz, 3H), 7.86 (d, *J* = 8.1 Hz, 2H), 7.80 (dd, *J* = 14.0, 12.6 Hz, 4H), 7.70 (d, *J* = 15.4 Hz, 2H), 7.56 – 7.48 (m, 4H), 7.44 (t, *J* = 7.0 Hz, 1H), 7.30 (d, *J* = 8.2 Hz, 1H), 6.85 (d, *J* = 8.1 Hz, 1H). ^{13}C NMR (101 MHz, DMSO-d_6) δ 188.80, 160.58, 144.87, 139.40, 137.19, 131.47, 129.50, 128.74, 127.41, 127.31, 126.23, 118.90, 116.24 . ESI-MS: *m/z* calcd for C$_{21}$H$_{16}$O$_2$ (M + H$^+$) 301.1, found 301.1.

(E) −1-([1,1′-biphenyl]-4-yl)-3-(4-hydroxy-3-methoxyphenyl)prop-2-en-1-one (compound **16**)

Yellow solid, yield: 75%. ^{1}H NMR (400 MHz, DMSO-d_6) δ 8.24 (d, *J* = 8.4 Hz, 2H), 7.86 (dd, *J* = 8.4, 3.1 Hz, 2H), 7.83 – 7.68 (m, 4H), 7.53 (dd, *J* = 12.2, 4.7 Hz, 3H), 7.45 (d, *J* = 8.7 Hz, 1H), 7.32 (d, *J* = 8.2 Hz, 1H), 6.91 – 6.83 (m, 1H), 3.90 (s, 3H). ^{13}C NMR (101 MHz, DMSO-d_6) δ 188.85, 148.42, 145.32, 144.62, 137.22, 129.55, 128.74, 127.40, 127.29, 126.71, 124.60, 119.09, 116.02, 112.16, 56.26 . ESI-MS: *m/z* calcd for C$_{21}$H$_{16}$O$_2$ (M + H$^+$) 330.1, found 330.1.

(E)-1-(2,4-dihydroxy-6-methoxyphenyl)-3-phenylprop-2-en-1-one (compound **17**)

Yellow solid, yield: 72%. ^{1}H NMR (400 MHz, DMSO-d_6) δ 14.40 (s, 1H), 10.37 (s, 1H), 7.90 (dd, *J* = 15.7, 7.0 Hz, 1H), 7.83 – 7.55 (m, 3H), 7.45 (s, 3H), 6.02 (d, *J* = 6.7 Hz, 1H), 3.87 (s, 3H), 3.72 (d, *J* = 5.8 Hz, 1H). ^{13}C NMR (101 MHz, DMSO-d_6) δ 191.99, 165.48, 163.83, 160.79, 141.64, 135.45, 130.61, 129.45, 128.72, 128.09, 107.22, 104.91, 91.47, 56.15 . ESI-MS: *m/z* calcd for C$_{16}$H$_{14}$O$_4$ (M + H$^+$) 270.0, found 270.0.

(E)-1-(2,4-dihydroxyphenyl)-3-(6-hydroxynaphthalen-2-yl)prop-2-en-1-one (compound **18**)

Yellow solid, yield: 85%. ^{1}H NMR (400 MHz, DMSO-d_6) δ 13.55 (s, 1H), 10.09 (s, 1H), 8.31 – 8.19 (m, 2H), 8.07 – 7.97 (m, 2H), 7.92 (d, *J* = 15.4 Hz, 1H), 7.84 (d, *J* = 8.8 Hz, 1H), 7.76 (d, *J* = 8.6 Hz, 1H), 7.23 – 7.09 (m, 2H), 6.45 (dd, *J* = 8.8, 2.0 Hz, 1H), 6.31 (d, *J* = 2.2 Hz, 1H). ^{13}C NMR (101 MHz, DMSO-d_6) δ 191.86, 166.25, 157.43, 144.75, 136.36,

133.45, 131.53, 130.86, 129.60, 127.86, 127.15, 125.20, 120.08, 119.73, 113.49, 109.49, 108.62, 103.02 . ESI-MS: *m/z* calcd for C$_{19}$H$_{14}$O$_4$ (M + H$^+$) 307.0, found 307.1.

(E)-1-(4-hydroxyphenyl)-3-(naphthalen-2-yl)prop-2-en-1-one (compound **19**)

Yellow solid, yield: 72%. ^{1}H NMR (400 MHz, DMSO-d_6) δ 10.46 (s, 1H), 8.53 (d, *J* = 15.3 Hz, 1H), 8.28 (d, *J* = 8.3 Hz, 1H), 8.22 (d, *J* = 7.2 Hz, 1H), 8.14 (d, *J* = 8.5 Hz, 2H), 8.08 – 7.95 (m, 3H), 7.63 (dq, *J* = 14.0, 6.7 Hz, 3H), 6.95 (d, *J* = 8.5 Hz, 2H). ^{13}C NMR (101 MHz, DMSO-d_6) δ 162.70, 139.06, 133.77, 131.98, 131.68, 130.91, 129.48, 129.17, 127.56, 126.67, 126.10, 125.87, 125.11, 123.40, 115.87 . ESI-MS: *m/z* calcd for C$_{19}$H$_{14}$O$_2$ (M + H$^+$) 275.1, found 275.1.

(E)-1-(2-hydroxy-4-methoxyphenyl)-3-(naphthalen-2-yl)prop-2-en-1-one (compound **20**)

Yellow solid, yield: 71%. ^{1}H NMR (400 MHz, DMSO-d_6) δ 13.41 (s, 1H), 8.67 (d, *J* = 15.2 Hz, 1H), 8.31 (t, *J* = 8.3 Hz, 3H), 8.15 – 8.06 (m, 2H), 8.03 (d, *J* = 8.0 Hz, 1H), 7.65 (dq, *J* = 16.4, 8.2, 7.7 Hz, 3H), 6.65 – 6.54 (m, 2H), 3.87 (s, 3H). ^{13}C NMR (101 MHz, DMSO-d_6) δ 166.11, 140.24, 133.24, 131.47, 129.24, 127.74, 126.75, 126.40, 126.09, 124.10, 123.34, 114.36, 107.94, 101.41, 56.22 . ESI-MS: *m/z* calcd for C$_{20}$H$_{16}$O$_3$ (M + H$^+$) 305.1, found 305.1.

(E)-1-(2-hydroxy-4-methoxyphenyl)-3-(6-hydroxynaphthalen-2-yl)prop-2-en-1-one (compound **21**)

Yellow solid, yield: 83%. ^{1}H NMR (400 MHz, DMSO-d_6) δ 13.60 (s, 1H), 10.10 (s, 1H), 8.34 (d, *J* = 9.1 Hz, 1H), 8.23 (s, 1H), 8.12 – 8.01 (m, 2H), 7.96 (d, *J* = 15.3 Hz, 1H), 7.84 (d, *J* = 8.8 Hz, 1H), 7.77 (d, *J* = 8.7 Hz, 1H), 7.23 – 7.09 (m, 2H), 6.64 – 6.50 (m, 2H), 3.87 (s, 3H). ^{13}C NMR (101 MHz, DMSO-d_6) δ 192.25, 166.33, 157.52, 145.26, 136.43, 133.03, 131.75, 130.90, 129.54, 127.16, 125.24, 120.00, 119.75, 114.32, 109.51, 107.80, 101.36, 56.19 . ESI-MS: *m/z* calcd for C$_{20}$H$_{16}$O$_4$ (M + H$^+$) 321.1, found 321.1.

(E)-1-([1,1′-biphenyl]-4-yl)-3-(naphthalen-2-yl)prop-2-en-1-one (compound **22**)

Yellow solid, yield: 88%. ^{1}H NMR (400 MHz, DMSO-d_6) δ 8.62 (d, *J* = 15.3 Hz, 1H), 8.31 (t, *J* = 6.7 Hz, 4H), 8.15 – 8.00 (m, 3H), 7.91 (d, *J* = 8.2 Hz, 2H), 7.80 (d, *J* = 7.4 Hz, 2H), 7.73 – 7.58 (m, 3H), 7.54 (t, *J* =
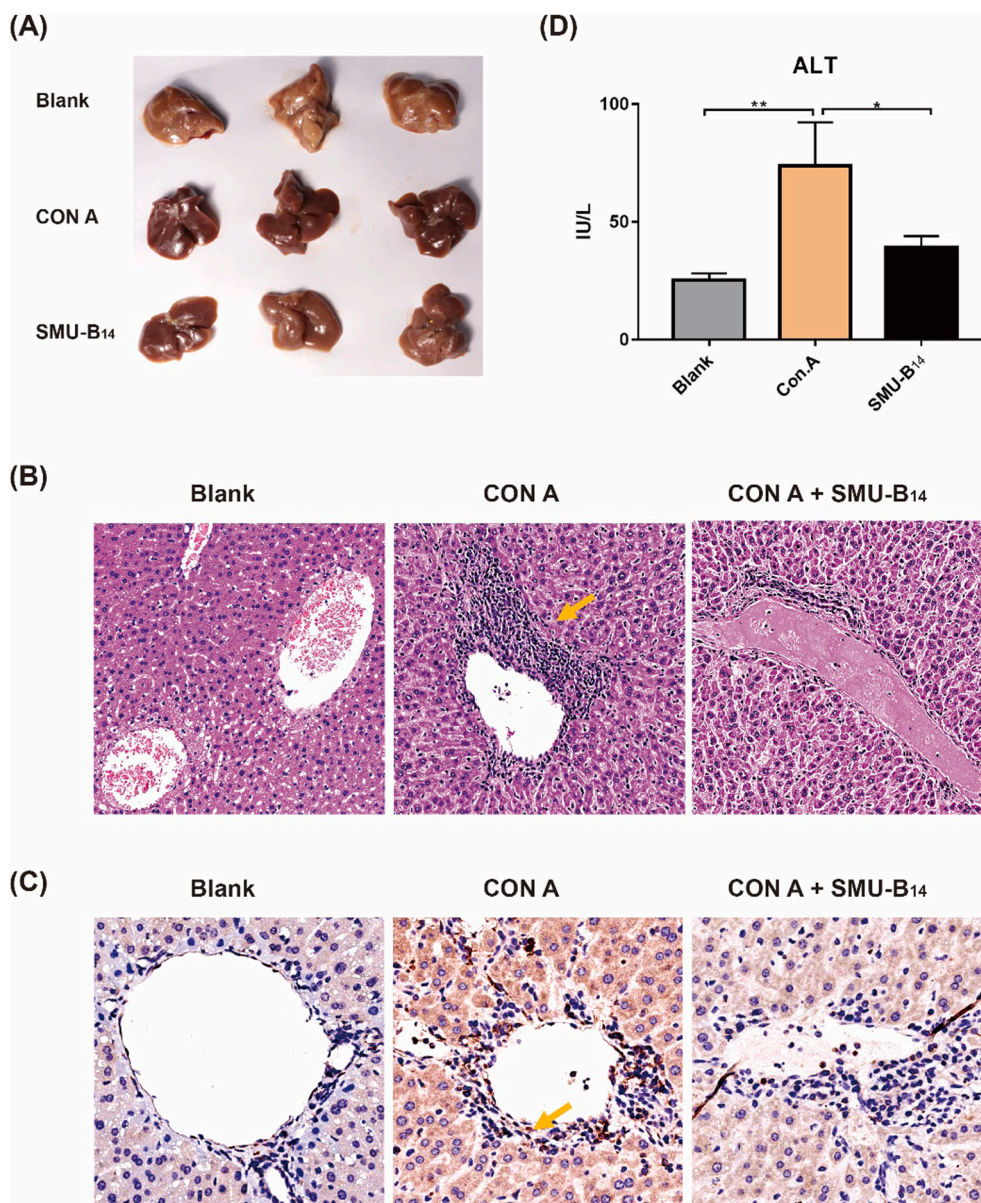
Fig. 6. SMU-B$_{14}$ reduced the serum ALT of acute hepatitis. (A) Photographic images of mouse livers. Photographs at 6 h display the gross pathology of livers from saline (Blank), Concanavalin A plus saline (CON A), Concanavalin A plus SMU-B$_{14}$ 50 mg/kg (SMU-B$_{14}$). (B) Histology of mouse livers at 6 h post injection. HE staining results of mouse livers were treated with saline (Blank), Concanavalin A plus saline (CON A), Concanavalin A plus SMU-B$_{14}$ 50 mg/kg (SMU-B$_{14}$). The neutrophil infiltration of liver tissues were shown by orange arrow. (C) Immunohistochemistry of iNOS from hepatic M$_1$-type macrophages. Immunohistochemistry results of iNOS of hepatic M$_1$-type macrophages were treated with saline (Blank), Concanavalin A plus saline (CON A), Concanavalin A plus SMU-B$_{14}$ 50 mg/kg (SMU-B$_{14}$). The M$_1$-type macrophage were shown by orange arrow. (D) C57BL/6J (WT) mice were treated i.p. with saline (Blank and CON A group) or 50 mg/kg SMU-B$_{14}$ (SMU-B$_{14}$ group). Then, all of mice received a tail intravenous injection with saline (Blank) or Concanavalin A (CON A, SMU-B$_{14}$) and were sacrificed at 6 h later. Serum ALT were tested. Data presented are mean ± SD and the figures shown are representative of three independent experiments. (*P < 0.05; **P < 0.01; ***P < 0.001). (For interpretation of the references to color in this figure legend, the reader is referred to the web version of this article.)

7.4 Hz, 2H), 7.46 (t, J = 7.2 Hz, 1H).^{13}C NMR (101 MHz, DMSO-d_6) δ 188.95, 140.25, 139.32, 133.79, 131.72, 131.64, 131.30, 129.80, 129.52, 129.23, 128.84, 127.69, 127.45, 126.74, 126.18, 126.13, 124.94, 123.40 . ESI-MS: m/z calcd for $C_{25}H_{18}O$ (M + H$^+$) 301.1, found 301.1. ESI-MS: m/z calcd for $C_{25}H_{18}O_1$ (M + H$^+$) 335.1, found 335.1.

(E)-1-([1,1′-biphenyl]-4-yl)-3-(6-hydroxynaphthalen-2-yl)prop-2-en-1-one (compound **23**)

Yellow solid, yield: 91%. ^{1}H NMR (400 MHz, DMSO) δ 10.06 (s, 1H), 8.28 (d, J = 7.9 Hz, 1H), 8.22 (s, 1H), 8.07 – 7.98 (m, 1H), 7.93 – 7.86 (m, 2H), 7.84 (d, J = 8.8 Hz, 1H), 7.78 (t, J = 9.6 Hz, 2H), 7.53 (t, J = 7.4 Hz, 1H), 7.44 (t, J = 7.3 Hz, 1H), 7.14 (d, J = 9.8 Hz, 1H). ^{13}C NMR (101 MHz, DMSO-d_6) δ 188.88, 157.38, 145.02, 144.80, 139.37, 137.04, 131.43, 130.84, 129.65, 129.51, 128.79, 127.44, 127.16, 125.14, 120.99, 119.71, 109.49 . ESI-MS: m/z calcd for $C_{25}H_{18}O_2$ (M + H$^+$) 351.1, found 351.1.

General procedure for synthesis of compound **24–39**

Compound **24–39** were synthesized as follow: (E)-1-(2,4-dihydroxyphenyl)-3-(4-hydroxyphenyl)prop-2-en-1-one (1 mmol) was added in Acetic acid (10 mL). Hydrazine hydrate (4 mmol) dissolved in Acetic acid (2 mL), was added in above solution drop wisely. The mixture was heated and refluxed at 80 °C for 10 h. After the reaction, saturated aqueous solution of NaHCO$_3$ was added in to adjust pH to 7. The mixture were extracted with ethyl acetate for three times, 10 mL for each. The organic layer was dried by anhydrous Na$_2$SO$_4$ and concentrated under reduced pressure. The residue was purified on a silica gel column (petroleum ether/ethyl acetate elute) to provide the compound.

1-(3-(2,4-dihydroxyphenyl)-5-(4-hydroxyphenyl)-4,5-dihydro-1H-pyrazol-1-yl)ethan-1-one (compound **24**)

White solid, yield: 56%. ^{1}H NMR (400 MHz, DMSO-d_6) δ 7.38 (s, 1H), 7.18 (d, J = 7.5 Hz, 2H), 7.09 (d, J = 8.0 Hz, 1H), 6.74 (d, J = 7.6 Hz, 2H), 6.32 (d, J = 8.1 Hz, 2H), 4.66 (t, J = 10.3 Hz, 1H), 3.44 (dd, J = 16.4, 10.5 Hz, 1H), 2.92 – 2.82 (m, 1H).^{13}C NMR (101 MHz, DMSO-d_6) δ 159.80, 158.95, 157.08, 153.75, 132.76, 129.23, 128.22, 115.56, 109.19, 107.45, 102.81, 61.90, 41.40 . ESI-MS: m/z calcd for $C_{17}H_{16}N_2O_4$ (M + H$^+$) 313.1, found 313.1.

1-(3-(2,4-dihydroxyphenyl)-5-(4-hydroxy-3-methoxyphenyl)-4,5-dihydro-1H-pyrazol-1-yl)ethan-1-one (compound **25**)

White solid, yield: 43%. ^{1}H NMR (400 MHz, DMSO-d_6) δ 10.26 (s, 1H), 10.03 (s, 1H), 8.98 (s, 1H), 7.35 (d, J = 9.1 Hz, 1H), 6.84 (d, J = 8.8 Hz, 1H), 6.59 (d, J = 4.9 Hz, 2H), 6.46 – 6.30 (m, 2H), 5.33 (dd, J = 11.5,
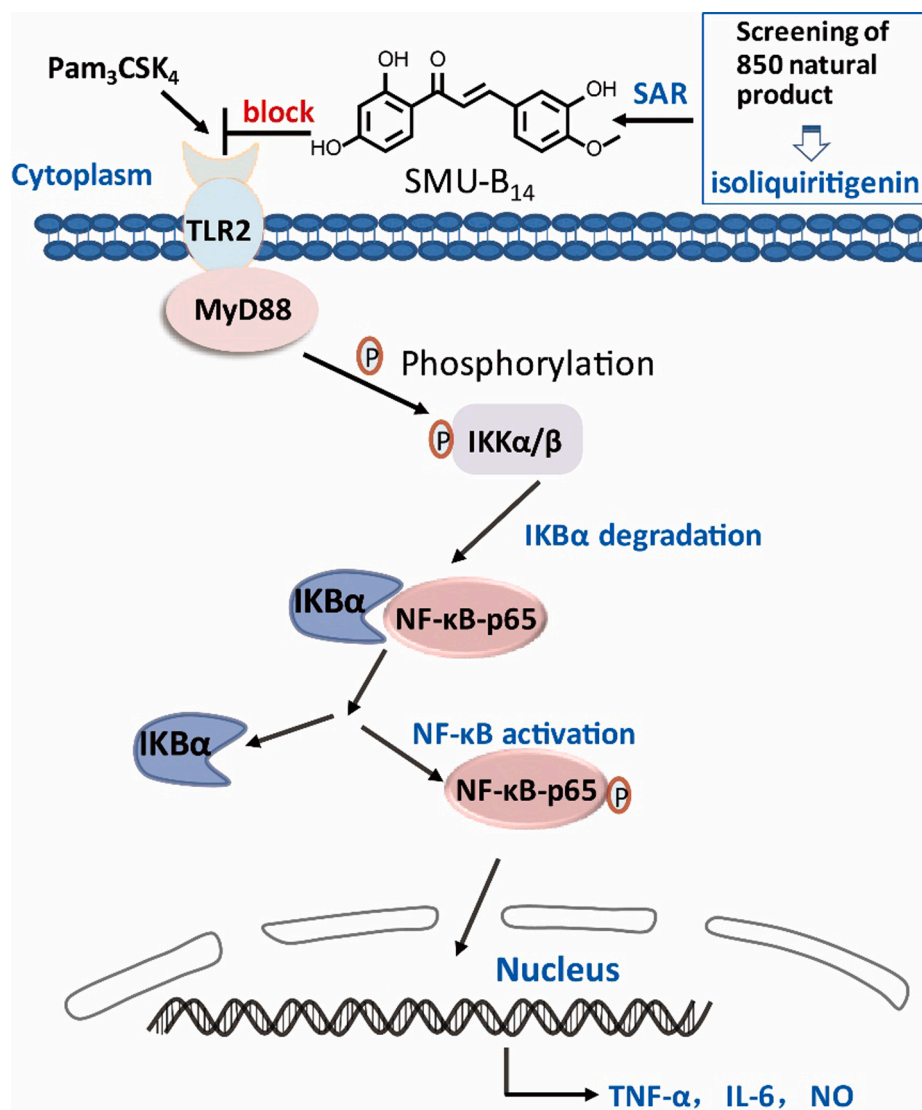
Fig. 7. SMU-B14 inhibited the activation of NF-κB pathway induced by TLR2. SMU-B14 blocked the interaction between TLR2 and its' ligand, and reduced the recruitment of MyD88, leading to the decreased phosphorylation of IKKα/β. As a result, the complex of IKBα and NF-κB-p65 failed to be degraded and phosphorylation, which resulted in the inhibition of inflammatory cytokines.

3.8 Hz, 1H), 3.92 – 3.79 (m, 1H), 3.73 (s, 3H), 3.16 (dd, J = 18.1, 3.9 Hz, 1H), 2.51 (s, 3H). ^{13}C NMR (101 MHz, DMSO-d_6) δ 166.73, 161.35, 158.98, 156.67, 147.05, 135.39, 130.81, 116.62, 112.80, 112.16, 108.19, 103.01, 57.86, 56.11, 43.63, 22.21 . ESI-MS: m/z calcd for $C_{18}H_{18}N_2O_5$ (M + H$^+$) 343.1, found 343.1.

1-(3-(2,4-dihydroxyphenyl)-5-(3-hydroxy-4-methoxyphenyl)-4,5-dihydro-1H-pyrazol-1-yl)ethan-1-one (compound **26**)

White solid, yield: 63%. ^{1}H NMR (400 MHz, DMSO-d_6) δ 10.17 (d, J = 83.3 Hz, 2H), 8.99 (s, 1H), 7.35 (d, J = 8.6 Hz, 1H), 6.85 (d, J = 8.0 Hz, 1H), 6.61 (s, 2H), 6.39 (s, 2H), 5.34 (d, J = 10.5 Hz, 1H), 3.94 – 3.80 (m, 1H), 3.76 (d, J = 21.3 Hz, 3H), 3.17 (d, J = 17.7 Hz, 1H), 2.25 (s, 3H). ^{13}C NMR (101 MHz, DMSO-d_6) δ 166.74, 161.37, 158.99, 156.68, 147.06, 135.38, 130.82, 116.64, 112.99, 108.35, 103.03, 57.86, 56.10, 43.61, 22.21 . ESI-MS: m/z calcd for $C_{18}H_{18}N_2O_5$ (M + H$^+$) 343.1, found 343.1.

1-(3,5-bis(4-hydroxyphenyl)-4,5-dihydro-1H-pyrazol-1-yl)ethan-1-one (compound **27**)

White solid, yield: 86%. ^{1}H NMR (400 MHz, DMSO-d_6) δ 9.95 (s, 1H), 9.32 (s, 1H), 7.62 (d, J = 8.6 Hz, 2H), 6.97 (d, J = 8.4 Hz, 2H), 6.83 (d, J = 8.6 Hz, 2H), 6.69 (d, J = 8.4 Hz, 2H), 5.39 (dd, J = 11.5, 4.0 Hz, 1H), 3.73 (dd, J = 17.8, 11.6 Hz, 1H), 3.03 (dd, J = 17.8, 4.1 Hz, 1H), 2.25 (s, 3H). ^{13}C NMR (101 MHz, DMSO-d_6) δ 167.25, 159.85, 156.84, 154.59, 133.34, 128.76, 127.07, 122.54, 115.96, 115.61, 59.07, 42.58, 22.15 . ESI-MS: m/z calcd for $C_{17}H_{16}N_2O_3$ (M + H$^+$) 297.1, found 297.0.

1-(5-(3-hydroxy-4-methoxyphenyl)-3-(4-hydroxyphenyl)-4,5-dihydro-1H-pyrazol-1-yl)ethan-1-one (compound **28**)

White solid, yield: 69%. ^{1}H NMR (400 MHz, DMSO-d_6) δ 9.99 (s, 1H), 8.98 (s, 1H), 7.62 (d, J = 8.3 Hz, 3H), 6.84 (d, J = 8.2 Hz, 3H), 6.58 (s, 2H), 5.36 (d, J = 11.3 Hz, 1H), 3.72 (s, 4H), 3.02 (d, J = 20.6 Hz, 1H), 2.26 (s, 3H). ^{13}C NMR (101 MHz, DMSO-d_6) δ 167.19, 159.88, 147.18, 147.04, 128.77, 126.87, 116.59, 115.97, 112.96, 112.80, 59.09, 56.11, 56.07, 42.61, 22.14 . ESI-MS: m/z calcd for $C_{18}H_{18}N_2O_4$ (M + H$^+$) 327.1, found 327.1.

1-(5-(4-hydroxy-3-methoxyphenyl)-3-(4-hydroxyphenyl)-4,5-dihydro-1H-pyrazol-1-yl)ethan-1-one (compound **29**)

White solid, yield: 77%. ^{1}H NMR (400 MHz, DMSO-d_6) δ 9.98 (s, 1H), 8.89 (s, 1H), 7.62 (d, J = 8.5 Hz, 2H), 6.93 – 6.66 (m, 4H), 6.53 (d, J = 8.0 Hz, 1H), 5.41 (dd, J = 11.5, 4.0 Hz, 1H), 3.73 (s, 3H), 3.12 – 3.01 (m, 1H), 2.27 (s, 3H). ^{13}C NMR (101 MHz, DMSO-d_6) δ 167.38, 159.84, 154.63, 147.91, 146.04, 133.93, 128.78, 122.55, 117.77, 115.85, 110.46, 59.33, 56.01, 42.67, 22.16 . ESI-MS: m/z calcd for $C_{18}H_{18}N_2O_4$ (M + H$^+$) 327.1, found 327.1.

1-(3-(4-hydroxyphenyl)-5-(4-(trifluoromethyl)phenyl)-4,5-dihydro-1H-pyrazol-1-yl)ethan-1-one (compound **30**)

White solid, yield: 57%. ^{1}H NMR (400 MHz, DMSO-d_6) δ 10.00 (s, 1H), 7.66 (dd, J = 29.8, 8.1 Hz, 4H), 7.41 (d, J = 8.0 Hz, 2H), 6.84 (d, J = 8.4 Hz, 2H), 5.60 (dd, J = 11.9, 4.7 Hz, 1H), 3.84 (dd, J = 18.0, 11.9 Hz, 1H), 3.12 (dd, J = 18.0, 4.7 Hz, 1H), 2.30 (s, 3H).^{13}C NMR (101 MHz, DMSO-d_6) δ 167.61, 160.00, 154.65, 147.51, 128.89, 126.80, 125.99, 122.22, 115.98, 59.26, 42.38, 22.03 . ESI-MS: m/z calcd for $C_{18}H_{15}F_3N_2O_2$ (M + H$^+$) 349.1, found 349.1.

1-(3-(2-hydroxy-4-methoxyphenyl)-5-(4-hydroxyphenyl)-4,5-dihydro-1H-pyrazol-1-yl)ethan-1-one (compound **31**)

White solid, yield: 73%. ^{1}H NMR (400 MHz, DMSO-d_6) δ 7.47 (d, J = 8.6 Hz, 1H), 6.99 (d, J = 8.4 Hz, 2H), 6.70 (d, J = 8.4 Hz, 2H), 6.58 – 6.44 (m, 2H), 5.38 (dd, J = 11.5, 3.9 Hz, 1H), 3.85 (dd, J = 18.2, 11.6 Hz, 1H), 3.77 (s, 3H), 3.21 (d, J = 14.2 Hz, 1H), 2.25 (s, 3H).^{13}C NMR (101 MHz, DMSO-d_6) δ 166.89, 162.66, 159.38, 157.03, 156.39, 132.91, 130.56, 127.10, 115.66, 109.72, 106.74, 101.66, 58.01, 55.73, 43.83, 22.24 . ESI-MS: m/z calcd for $C_{18}H_{18}N_2O_4$ (M + H$^+$) 327.1, found 327.1.

1-(3-(2-hydroxy-4-methoxyphenyl)-5-(3-hydroxy-4-methoxyphenyl)-4,5-dihydro-1H-pyrazol-1-yl)ethan-1-one (compound **32**)

White solid, yield: 74%. ^{1}H NMR (400 MHz, DMSO-d_6) δ 10.38 (s, 1H), 8.91 (s, 1H), 7.46 (s, 1H), 6.74 (d, J = 36.6 Hz, 2H), 6.54 (d, J = 6.4 Hz, 3H), 5.39 (dd, J = 11.4, 3.7 Hz, 1H), 3.86 (dd, J = 18.1, 11.7 Hz, 1H), 3.76 (d, J = 15.7 Hz, 6H), 3.23 (dd, J = 18.2, 3.9 Hz, 1H), 2.27 (s, 3H).^{13}C NMR (101 MHz, DMSO-d_6) δ 167.03, 162.67, 158.90, 156.37, 147.96, 146.15, 133.52, 130.69, 117.86, 115.86, 110.54, 107.02, 101.58, 58.24, 56.04, 55.79, 43.74, 22.26 . ESI-MS: m/z calcd for $C_{19}H_{20}N_2O_5$ (M + H$^+$) 357.1, found 357.1.

1-(5-(4-hydroxy-3-methoxyphenyl)-3-(2-hydroxy-4-methoxyphenyl)-4,5-dihydro-1H-pyrazol-1-yl)ethan-1-one (compound **33**)

White solid, yield: 68%. ^{1}H NMR (400 MHz, DMSO-d_6) δ 10.38 (s, 1H), 8.95 (d, J = 27.1 Hz, 1H), 7.45 (d, J = 8.3 Hz, 1H), 6.89 – 6.76 (m, 1H), 6.71 (d, J = 8.0 Hz, 1H), 6.63 – 6.50 (m, 3H), 5.51 – 5.23 (m, 1H), 3.87 (dd, J = 13.7, 4.9 Hz, 1H), 3.76 (d, J = 14.9 Hz, 6H), 3.29 – 3.15 (m, 1H), 2.27 (s, 3H).^{13}C NMR (101 MHz, DMSO-d_6) δ 167.03, 162.70, 158.91, 156.37, 133.52, 130.69, 117.86, 116.64, 115.87, 113.02, 110.54, 109.58, 107.01, 101.58, 58.24, 56.04, 55.78, 43.72, 22.26 . ESI-MS: m/z calcd for $C_{19}H_{20}N_2O_5$ (M + H$^+$) 357.1, found 357.1.

1-(3-(2-hydroxy-4-methoxyphenyl)-5-(3,4,5-trimethoxyphenyl)-4,5-dihydro-1H-pyrazol-1-yl)ethan-1-one(compound **34**)

White solid, yield: 82%. ^{1}H NMR (400 MHz, DMSO-d_6) δ 10.36 (s, 1H), 7.45 (d, J = 9.3 Hz, 1H), 6.60 – 6.45 (m, 4H), 5.42 (dd, J = 11.6, 4.6 Hz, 1H), 3.93 – 3.85 (m, 1H), 3.78 (s, 3H), 3.74 (s, 6H), 3.64 (s, 3H), 3.25 (dd, J = 18.2, 4.7 Hz, 1H), 2.30 (s, 3H).^{13}C NMR (101 MHz, DMSO-d_6) δ 167.33, 162.69, 158.88, 156.26, 153.46, 138.39, 136.97, 130.70, 109.60, 107.00, 102.98, 101.58, 60.32, 58.69, 56.29, 55.78, 43.85, 22.23 . ESI-MS: m/z calcd for $C_{21}H_{24}N_2O_6$ (M + H$^+$) 401.1, found 401.1.

1-(3-([1,1′-biphenyl]-4-yl)-5-(4-hydroxy-3-methoxyphenyl)-4,5-dihydro-1H-pyrazol-1-yl)ethan-1-one (compound **35**)

White solid, yield: 72%. ^{1}H NMR (400 MHz, DMSO-d_6) δ 8.92 (s, 1H), 7.87 (d, J = 8.1 Hz, 2H), 7.75 (dd, J = 19.5, 7.9 Hz, 4H), 7.50 (t, J = 7.5 Hz, 2H), 7.41 (t, J = 7.2 Hz, 1H), 6.79 (s, 1H), 6.72 (d, J = 8.1 Hz, 1H), 6.57 (d, J = 7.9 Hz, 1H), 5.48 (dd, J = 11.5, 4.1 Hz, 1H), 3.83 (dd, J = 17.9, 11.8 Hz, 1H), 3.75 (s, 3H), 3.17 (dd, J = 17.9, 4.2 Hz, 1H), 2.33 (s, 3H).^{13}C NMR (101 MHz, DMSO-d_6) δ 167.76, 154.23, 133.79, 129.44, 128.36, 127.62, 127.33, 127.08, 117.90, 115.89, 110.51, 60.16, 56.02, 42.53, 22.21 . ESI-MS: m/z calcd for $C_{24}H_{22}N_2O_3$ (M + H$^+$) 387.1, found 387.1.

1-(3-(2,4-dihydroxy-6-methoxyphenyl)-5-phenyl-4,5-dihydro-1H-pyrazol-1-yl)ethan-1-one (compound **36**)

White solid, yield: 44%. ^{1}H NMR (400 MHz, DMSO-d_6) δ 11.19 (s, 1H), 10.08 (s, 1H), 7.34 (t, J = 7.3 Hz, 2H), 7.23 (dd, J = 24.6, 7.3 Hz, 3H), 6.01 (d, J = 4.2 Hz, 2H), 5.41 (dd, J = 11.6, 3.9 Hz, 1H), 3.95 (dd, J = 18.8, 11.7 Hz, 1H), 3.70 (s, 3H), 3.21 (dd, J = 18.8, 4.1 Hz, 1H), 2.24 (s, 3H).^{13}C NMR (101 MHz, DMSO-d_6) δ 166.67, 161.68, 160.98,

160.38, 156.07, 142.86, 129.05, 127.57, 125.78, 98.17, 96.28, 92.02, 57.79, 56.02, 46.96, 22.15 . ESI-MS: m/z calcd for $C_{18}H_{18}N_2O_4$ (M + H$^+$) 327.1, found 327.1.

1-(5-(4-hydroxy-3-methoxyphenyl)-3-(2-hydroxy-4-(trifluoromethyl)phenyl)-4,5-dihydro-1H-pyrazol-1-yl)ethan-1-one (compound **37**)

White solid, yield: 44%. ^{1}H NMR (400 MHz, DMSO-d_6) δ 10.72 (s, 1H), 8.92 (s, 1H), 7.85 (d, J = 8.1 Hz, 1H), 7.25 (d, J = 7.7 Hz, 2H), 6.80 (s, 1H), 6.71 (d, J = 8.1 Hz, 1H), 6.58 (d, J = 8.0 Hz, 1H), 5.44 (dd, J = 11.6, 4.3 Hz, 1H), 3.92 (dd, J = 18.4, 11.9 Hz, 1H), 3.75 (s, 3H), 3.30 – 3.24 (m, 1H), 2.30 (s, 3H).^{13}C NMR (101 MHz, DMSO-d_6) δ 167.72, 157.13, 154.33, 147.98, 146.19, 133.51, 130.43, 121.27, 117.95, 116.17, 115.86, 110.49, 59.22, 56.03, 44.41, 22.25 . ESI-MS: m/z calcd for $C_{19}H_{17}F_3N_2O_4$ (M + H$^+$) 395.1, found 395.1.

1-(3-(4-hydroxyphenyl)-5-(naphthalen-2-yl)-4,5-dihydro-1H-pyrazol-1-yl)ethan-1-one (compound **38**)

White solid, yield: 55%. ^{1}H NMR (400 MHz, DMSO-d_6) δ 9.98 (s, 1H), 8.17 (d, J = 8.2 Hz, 1H), 7.99 (d, J = 7.9 Hz, 1H), 7.84 (d, J = 8.2 Hz, 1H), 7.61 (h, J = 7.1 Hz, 4H), 7.44 (t, J = 7.7 Hz, 1H), 7.12 (d, J = 7.1 Hz, 1H), 6.81 (d, J = 8.5 Hz, 2H), 6.25 (dd, J = 11.6, 4.0 Hz, 1H), 4.05 (dd, J = 17.6, 11.9 Hz, 1H), 2.99 (dd, J = 17.7, 4.3 Hz, 1H), 2.40 (s, 3H).^{13}C NMR (101 MHz, DMSO-d_6) δ 167.59, 159.93, 137.60, 134.14, 129.16, 128.83, 127.87, 126.74, 126.24, 125.94, 123.79, 115.96, 57.03, 42.47, 22.16 . ESI-MS: m/z calcd for $C_{21}H_{18}N_2O_2$ (M + H$^+$) 331.1, found 331.1.

General procedure for synthesis of compound **39–40**

Compound **39–40** were synthesized as follow: (E)-1-(2-hydroxy-4-methoxyphenyl)-3-(4-hydroxyphenyl)prop-2-en-1-one (0.37 mmol) and urea (3.71 mmol) were added in hydrochloric acid 1,4-dioxane (4 mL). The mixture was heated and refluxed for 12 h. After the reaction, saturated aqueous solution of NaHCO$_3$ was added in to adjust pH to 7. The mixture liquor were extracted with ethyl acetate in three times, 10 mL for each. The organic layer was dried with anhydrous Na$_2$SO$_4$ and concentrated under reduced pressure. The residue was purified on a silica gel column (petroleum ether/ethyl acetate elute) to provide compound.

4-(2-hydroxy-4-methoxyphenyl)-6-(3-hydroxy-4-methoxyphenyl)-5,6-dihydropyrimidin-2(1H)-one (compound **39**)

White solid, yield: 42%. ^{1}H NMR (400 MHz, Chloroform-d) δ 7.90 (d, J = 8.8 Hz, 1H), 7.00 (d, J = 14.4 Hz, 3H), 6.69 – 6.60 (m, 1H), 6.52 (s, 1H), 5.73 (d, J = 8.6 Hz, 1H), 5.41 (dd, J = 13.3, 2.3 Hz, 1H), 3.96 (s, 3H), 3.86 (s, 3H), 3.08 (dd, J = 16.8, 13.4 Hz, 1H), 2.83 (dd, J = 16.8, 2.7 Hz, 1H).^{13}C NMR (101 MHz, Chloroform-d) δ 190.69, 166.11, 163.47, 146.68, 146.09, 130.60, 128.70, 119.57, 114.76, 114.47, 110.16, 108.74, 100.88, 80.05, 55.95, 55.59, 44.28 . ESI-MS: m/z calcd for $C_{18}H_{18}N_2O_5$ (M + H$^+$) 343.1, found 343.1.

4-(2-hydroxy-4-methoxyphenyl)-6-(4-hydroxyphenyl)-5,6-dihydropyrimidin-2(1H)-one (compound **40**)

White solid, yield: 44%. ^{1}H NMR (400 MHz, DMSO-d_6) δ 9.57 (s, 1H), 7.72 (d, J = 8.8 Hz, 1H), 7.35 (d, J = 8.4 Hz, 2H), 6.80 (d, J = 8.5 Hz, 2H), 6.66 (dd, J = 8.8, 2.3 Hz, 1H), 6.60 (d, J = 2.2 Hz, 1H), 5.50 (dd, J = 13.0, 2.5 Hz, 1H), 3.81 (s, 3H), 3.18 (dd, J = 16.8, 13.0 Hz, 1H), 2.67 (dd, J = 16.8, 2.9 Hz, 1H).^{13}C NMR (101 MHz, DMSO-d_6) δ 190.76, 166.02, 163.65, 158.06, 129.53, 128.70, 128.38, 115.53, 114.82, 110.24, 101.38, 79.60, 56.20, 43.50. ESI-MS: m/z calcd for $C_{17}H_{16}N_2O_4$ (M + H$^+$) 313.1, found 313.1.

4.2. Biology assays

4.2.1. Preparation of peritoneal macrophage

Peritoneal macrophage were obtained by peritoneal lavage from 6 to 8 week old C57BL/6 mice (purchased from the Laboratory Animal Center of Southern Medical University) 4d after i.p injection of 3 mL 4% sterile thioglycollate. Cells were washed with PBS three times and cultured in RPMI 1640 [supplemented with 10% FBS, penicillin (100 U/ml), and streptomycin (100 mg/ml)]. The cells were used in subsequent

experiment.

4.2.2. Preparation of bone Marrow-Derived dendritic cells (BMDC)

Total cells were harvested by flushing cells from femurs and tibiae of C57BL/6 mice and cultured with RPMI 1640 [supplemented with 10% FBS, penicillin (100 U/ml), and streptomycin (100 mg/ml)] for 2 h in petri dish. The supernatant was transferred to new petri dish to remove adherent cell and murine IL-4(10 ng/mL), murine GM-CSF (40 ng/mL) were added in. After 7 days incubation, BMDC were collected after cell culture medium was changed and the unattached cells were removed.

4.2.3. Griess method for NO test

The inhibition release of NO was measured by Griess reagent. Briefly, dissolving 85% strong phosphoric acid (3 mL) and sulfanilic acid (0.5 g) in 40 mL water to make 50 mL obtained substrate solution A, then dissolving naphthyl ethyl-enediamine dihydrochloride (0.05 g) in 50 mL water to make substrate solution B. Murine primary peritoneal macrophages cells were seeded in a 384 well plastic plate (Thermo Scientific) at a density of 3×10^4 per well, treated with IFN-γ (final conc. 40 ng/mL), Pam$_3$CSK$_4$ (InviviGen, final conc. 100 ng/mL) and indicated concentration compounds. After incubation (37 °C, 5% CO$_2$) for 24 h later, the equal volume of substrate solution A and substrate solution B was added in. Ten minutes later, the plate was measured at an absorbance of 560 nm through a microplate reader (Thermo Scientific).

4.2.4. Cell toxicity assays

Murine primary peritoneal macrophages cells (3×10^4 cells per well) were seeded in 96 well plastic plate with 100 μL RPMI 1640 [supplemented with 10% FBS, penicillin (100 U/ml), and streptomycin (100 mg/ml)] and incubated at 37 °C overnight. After that, indicated concentration compounds were added to 200 μL totally and incubated (37℃, 5% CO$_2$) for another 24 h. Twenty μL (5 mg/mL) MTT [3-(4,5-dimethylthiazol-2-yl)-2,5-diphenyltetrazolium bromide] were added into each well and incubated (37℃, 5% CO$_2$) for 4 h. The supernatant was removed totally and 50 μL DMSO were added in and shaken continuously for 10 min. In the end, the plate was measured at an absorbance of 560 nm through a plate reader (Thermo Scientific).

4.2.5. Cytokine ELISA assays

Raw 264.7 cells, Murine Peritoneal Macrophage, Murine Bone Marrow-Derived Dendritic cells or human PBMC cells were seeded in 12-well plates at a density of 0.5×10^6 cells per well with 1 mL of RPMI 1640 [supplemented with 10% FBS, penicillin (100 U/ml), and streptomycin (100 mg/ml)]. The cells were treated with indicated concentrations of SMU-B$_{14}$ and Pam$_3$CSK$_4$ (InviviGen, 50 ng/mL in Raw 264.7, 70 ng/mL in PBMC, 100 ng/mL in others) as positive control and incubated (37℃, 5% CO$_2$) for 24 h. The cell culture supernatants were collected and frozen at −80 °C until measurement. THP-1 cells at a density of 2.5×10^5 cells/mL were differentiated by treatment with 100 nM PMA (Sigma) in RPMI 1640 [supplemented with 10% FBS, penicillin (100 U/ml), and streptomycin (100 mg/ml)]. After that, cells were washed with PBS three times and cultured in fresh RPMI 1640 [supplemented with 10% FBS, penicillin (100 U/ml), and streptomycin (100 mg/ml)] for 24 h. The cell culture supernatants were collected and froze at −80 °C until measurement. The level of cytokine TNF-α, IL-6, IL-1β were determined using recombinant cytokine standards, cytokine-specific capture antibodies and detection antibodies according to the commercially available ELISA kit (BD Biosciences) with each sample for duplicate.

4.2.6. Western Blot analysis

Raw 264.7 cells were seeded in 6-well plate (Thermo Scientific) at density of 1.5×10^6 per well in 2 mL DMEM [supplemented with 10% FBS, penicillin (100 U/ml), and streptomycin (100 mg/ml)] and incubated (37 °C, 5% CO$_2$) for 24 h. Replaced the medium with DMEM only to 2 mL totally and treated the cells with different concentration of SMU-B$_{14}$ and Pam$_3$CSK$_4$ (InviviGen, 300 ng/mL) incubated for 12 h. The cells were harvested and lysed with 150 μL cell lysis buffers (PIPA mixed with PMSF at ratio of 50:1 before use, Boster). Cell lysates of equal amount were denatured, separated by sodium dodecyl sulfate polyacrylamide gel electrophoresis (SDS-PAGE), and transferred to polyvinylidene fluoride (PVDF) membrane (Millipore, IPVH00010). Nonspecific reactivity was blocked in TBST with 5% skim milk (BD, 6342932) for 1 h at room temperature, and then incubated with the primary antibody of TLR2 and GAPDH overnight at 4 °C. Membranes were then probed with the primary antibodies overnight at 4 °C and secondary antibodies at room temperature for 1 h. Reactive protein was detected by ECL chemiluminescence system (ProteinSimple, FlourChem R).

Murine Peritoneal Macrophage cells were seeded in 6-well plate (Thermo Scientific) at density of 2×10^6 per well in 2 mL RPMI 1640 [supplemented with 10% FBS, penicillin (100 U/ml), and streptomycin (100 mg/ml)] and incubated overnight. Replaced the medium with RPMI 1640 medium only to 2 mL totally and pretreated the cells with different concentration of SMU-B$_{14}$ for 1 h. Pam$_3$CSK$_4$ (InviviGen, 300 ng/mL) was added in and incubated from 15 min to 30 min. The cells were harvested and lysed with 150 mL cell lysis buffers (containning protease inhibitor and phosphoprotease inhibitor). Cell lysates of equal amount were denatured, separated by sodium dodecyl sulfate polyacrylamide gel electrophoresis (SDS-PAGE), and transferred to polyvinylidene fluoride (PVDF) membrane (Millipore, IPVH00010). Nonspecific reactivity was blocked in TBST with 5% skim milk (BD, 6342932) for 1 h at room temperature, and then incubated with the primary antibody of phosphorylated p65, phosphorylated p38, phosphorylated IKKα/β, IKBα and GAPDH overnight at 4 °C. Membranes were then probed with the primary antibodies overnight at 4 °C and secondary antibodies at room temperature for 1 h. Reactive protein was detected by ECL chemiluminescence system (ProteinSimple, FlourChem R).

4.2.7. Peritoneal macrophage phenotype assay

Murine Peritoneal Macrophage cells were seeded in 12-well plate (Thermo Scientific) at density of 1×10^6 per well in 1 mL RPMI 1640 [supplemented with 10% FBS, penicillin (100 U/ml), and streptomycin (100 mg/ml)] and incubated overnight. Peritoneal macrophage were treated with Pam$_3$CSK$_4$ (InviviGen, 100 ng/mL), murine IFN-γ (40 ng/mL) and indicated SMU-B$_{14}$ for 24 h. Treatment with LPS (InviviGen, 100 ng/mL) and murine IFN-γ (40 ng/mL) was considered as positive M1 phenotype. Cells were collected into centrifuge tube after trypsinization and carefully aspirated the supernatant after centrifugation at 300 g for 5 min. The cells were washed twice with PBS and stained with a mixture of antibodies for 30 min, including anti-mouse CD86-PE-Cy7 (BD Biosciences), anti-mouse CD11b-FITC (BD Biosciences). After the incubation, the tube was centrifuged at 300g for 5 min and washed twice withPBS. Stained cells were analyzed with flow cytometer (FACScanto II,0 BD) and the flow cytometry data were analyzed using FlowJo software.

4.2.8. Acute hepatitis assays

Male C57BL/6 mice with weight ranged from 20 to 22 g were purchased from the Laboratory Animal Center of Southern Medical University at 6–8 weeks old. Before the beginning of the study, the mice were allowed to adapt to the environment for 7 d. All of mice were raised under standard conditions with a 12 h light–dark cycle at 22 ± 1 °C and $55 \pm 5\%$ humidity with food and water provided ad libitum. Male C57BL/6 mice were randomly divided into three groups of three animals each. Subsequently, Mice were treated with saline, SMU-B$_{14}$ (50 mg/kg) 0.5 h before 100 μL of Concanavalin A (10 mg/kg) suspended in saline or saline was administered by tail intravenous injection. Six hours later, all mice were sacrificed and their blood were collected for ALT assay. The mice liver were dissected and soaked in formalin for HE staining and immunohistochemistry.

4.2.9. ALT assays

All mice blood samples were collected from acute hepatitis assays. Blood samples were placed in a centrifuge tubes at room temperature for 1 h and then centrifuged by 8000 rpm for 10 min. After centrifugation, the supernatant was collected for Alanine aminotransferase Assay kit (Nanjing Jiancheng Bioengineering Institute).

4.2.10. Histological analysis

Tissue slices were fixed in 10% formalin for 3 days, decalcified overnight and embedded in paraffin and sectioned into 4 μm tissue sections. Tissue sections were stained with hematoxylin and eosin before being examined under a BX60 microscope (Olympus, Melville, NY, USA) for pathological changes.

4.2.11. Immunohistochemical analysis

The liver tissue, preserved in 2.5% glutaraldehyde-polyoxymethylene solution, were dehydrated and embedded in paraffin following routine methods. The paraffin sections were removed paraffin, and then immersed in the distilled water following routine methods. Afterwards, Rinsing the paraffin sections (3×5 min) in PBS-T (0.01 M PBS pH 7.4: KH_2PO_4 0.02%, N_2HPO_4 0.29%, KCl 0.02%,0.8% NaCl, 0.05% BSA, Tween-20 0.05%, 0.0015% TritonX-100), and then blocked with 3% peroxide-methanol at room temperature for endogenous peroxidase ablation. All following steps were carried out in a moist chamber:

(1) Incubation with blocking buffer (normal goat serum at room temperature for 20 min).

(2) Discarding the serum and droping the rabbit anti-mouse iNOs with diluted in PBS(0.01 M PBS, pH 7.4) .

(3) incubating the sections for two hours at 37 °C.

(4) Rinsing in PBS-T(three times, 5 min each).

(5)Droping the goat anti-rabbit IgG(IgG /Bio),and incubating the sections for 30 min at 37 °C.

(6) Rinsing in PBS-T(three times, 5 min each).

(7) Incubation with the S-A/ HRP at 37 °C for 30 min.

(8) Rinsing (three times, 5 min each) in PBS-T.

(9) Colouration with 3,3-diaminobenzidin (DAB), kept at room temperature without light for 10 min.

(10)Finishing colouration with the distilled water.

(11)Hematoxylin stained.

(12) Dehydration, clearing and mounting with neutral gums.

Declaration of Competing Interest

The authors declare that they have no known competing financial interests or personal relationships that could have appeared to influence the work reported in this paper.

Acknowledgments

Appendix A. Supplementary material

Supplementary data to this article can be found online at https://doi.org/10.1016/j.bioorg.2021.105043.

References

[1] R.J.D. Dalio, D.M. Magalhães, C.M. Rodrigues, G.D. Arena, T.S. Oliveira, R. R. Souza-Neto, S.C. Picchi, P.M.M. Martins, P.J.C. Santos, H.J. Maximo, I. S. Pacheco, A.A.D. Souza, M.A. Machado, PAMPs, PRRs, effectors and R-genes associated with citrus-pathogen interactions, Ann. Bot 5 (2017) 749–774, https://doi.org/10.1093/aob/mcw238.

[2] R. Hatinguais, J.A. Willment, G.D. Brown, PAMPs of the Fungal Cell Wall and Mammalian PRRs, Curr. Top. Microbiol. Immunol 425 (2020) 187–223, https://doi.org/10.1007/82_2020_201.

[3] S.Y. Cai, G.Z. Zhu, X.H. Cen, J.J. Bi, J.R. Zhang, X.S. Tang, K. Chen, K. Cheng, Synthesis, structure-activity relationships and preliminary mechanism study of N-benzylideneaniline derivatives as potential TLR2 inhibitors, Bioorg. Med. Chem. 8 (2018) 2041–2050, https://doi.org/10.1016/j.bmc.2018.03.001.

[4] S. Federico, L. Pozzetti, A. Papa, G. Carullo, S. Gemma, S. Butini, G. Campiani, N. Relitti, Modulation of the Innate Immune Response by Targeting Toll-like Receptors: A Perspective on their Agonists and Antagonists, J. Med. Chem. 63 (2020) 13466–13513, https://doi.org/10.1021/acs.jmedchem.0c01049.

[5] S. De, H. Zhou, D. DeSantis, C.M. Croniger, X.X. Li, G.R. Stark, Erlotinib protects against LPS-induced endotoxicity because TLR4 needs EGFR to signal, Proc. Natl. Acad. Sci. 31 (2015) 9680–9685, https://doi.org/10.1073/pnas.1511794112.

[6] C.L. Li, L.X. Ma, Y.L Liu, Z.Z. Li, Q.B. W, Z. Chen, X. G, X.Y. Han, J.D. Sun, Z.F. Li, TLR2 promotes development and progression of human glioma via enhancing autophagy, Gene. 700 (2019) 52-59. DOI: 10.1016/j.gene.2019.02.084.

[7] M.Y. Dai, F.F. Chen, Y. Wang, M.Z. Wang, Y.X. Lv, R.Y. Liu, Particulate matters induce acute exacerbation of allergic airway inflammation via the TLR2/NF-κB/NLRP3 signaling pathway, Toxicol. Lett. 321 (2020) 146–154, https://doi.org/10.1016/j.toxlet.2019.12.013.

[8] Y. Wang, L.J. Su, M.D. Morin, B.T. Jones, Y. Mifune, H.X. Shi, K,W, Wang, X.M. Zhan, A.J. Liu, J.H. Wang, X.H. Li, M. Tang, S. Ludwig, S. Hildebrand, K.J. Zhou, D. J. Siegwart, E.M.Y. Moresco, H. Zhang, D.L. Boger, B. Beutler, Adjuvant effect of the novel TLR1/TLR2 agonist Diprovocim synergizes with anti-PD-L1 to eliminate melanoma in mice, Proc. Natl. Acad. Sci. 37 (2018) E8698-E8706. DOI: 10.1073/pnas.1809232115.

[9] B.J. Ge, P. Zhao, H.T. Li, R. Sang, M. Wang, H.Y. Zhou, X.M. Zhang, Taraxacum mongolicum protects against Staphylococcus aureus-infected mastitis by exerting anti-inflammatory role via TLR2-NF-κB/MAPKs pathways in mice, J. Ethnopharmacol. (2020), 113595, https://doi.org/10.1016/j.jep.2020.113595.

[10] L.J. Su, Y. Wang, J.M. Wang, Y. Mifune, M.D. Morin, B.T. Jones, E.M.Y. Moresco, D.L. Boger, B. Beutler, H. Zhang, Structural Basis of TLR2/TLR1 Activation by the Synthetic Agonist Diprovocim, J. Med. Chem. 6 (2019) 2938–2949, https://doi.org/10.1021/acs.jmedchem.8b01583.

[11] X.H. Cen, G.Z. Zhu, J.J. Yang, J.Y. Guo, J.B. Jin, K.S. Nandakumar, W. Yang, H. Yin, S.W. Liu, K. Cheng, TLR1/2 Specific Small-Molecule Agonist Suppresses Leukemia Cancer Cell Growth by Stimulating Cytotoxic T Lymphocytes, Adv. Sci. 10 (2019) 1802042, https://doi.org/10.1002/advs.201802042.

[12] H. Lu, Y. Yang, E. Gad, C. Inatsuka, C.A. Wenner, M.L. Disis, L.J. Standish, TLR2 Agonist PSK Activates Human NK Cells and Enhances the Antitumor Effect of HER2-Targeted Monoclonal Antibody Therapy, Clin. Cancer Res. 17 (2011) 6742–6753, https://doi.org/10.1158/1078-0432.CCR-11-1142.

[13] S.B. Rangasamy, M. Jana, A. Roy, G.T. Corbett, M. Kundu, S. Chandra, S. Mondal, S. Dasarathi, E.J. Mufson, R.K. Mishra, C. Luan, D.A. Bennett, K. Pahan, Selective disruption of TLR2-MyD88 interaction inhibits inflammation and attenuates Alzheimer's pathology, J. Clin. Invest. 128 (2018) 4297–4312, https://doi.org/10.1172/JCI96209.

[14] S.K. Whiteside, J.P. Snook, Y. Ma, F.L. Sonderegger, C. Fisher, C. Petersen, J. F. Zachary, J.L. Round, M.A. Williams, J.J. Weis, IL-10 Deficiency Reveals a Role for TLR2-Dependent Bystander Activation of T Cells in Lyme Arthritis, J. Immunol. 200 (2018) 1457–1470, https://doi.org/10.4049/jimmunol.1701248.

[15] W. Wang, Z. Deng, H. Wu, Q. Zhao, T. Li, W. Zhu, X. Wang, L. Tang, C. Wang, S. Cui, H. Xiao, J. Chen, A small secreted protein triggers a TLR2/4-dependent inflammatory response during invasive Candida albicans infection, Nat. Commun. 10 (2019) 1015, https://doi.org/10.4049/jimmunol.1701248.

[16] K. Cheng, X. Wang, S. Zhang, H. Yin, Discovery of small-molecule inhibitors of the TLR1/TLR2 complex, Angew. Chem. Int. Ed. 51 (2012) 12246–12249, https://doi.org/10.1002/anie.201204910.

[17] P. Mistry, M.H.W. Laird, R.S. Schwarz, S. Greene, T. Dyson, G.A. Snyde, T.S. Xiao, J. Chauhan, S. Fletcher, V.Y. Toshchakov, A.D.M. Jr, S.N. Vogel, Inhibition of TLR2 signaling by small molecule inhibitors targeting a pocket within the TLR2 TIR domain, Proc. Natl. Acad. Sci. 17 (2015) 5455–5460, https://doi.org/10.1073/pnas.1422576112.

[18] J.J. Bi, W.Q. Wang, J.X. Du, K. Chen, K. Cheng, Structure-activity relationship study and biological evaluation of SAC-Garlic acid conjugates as novel anti-inflammatory agents, Eur. J. Med. Chem. 179 (2019) 233–245, https://doi.org/10.1016/j.ejmech.2019.06.059.

[19] M. Grabowski, M.S. Murgueitio, M. Bermudez, J. Rademann, G. Wolber, G. Weindl, Identification of a pyrogallol derivative as a potent and selective human TLR2 antagonist by structure-based virtual screening, Biochem. Pharmacol. 154 (2018) 148–160, https://doi.org/10.1016/j.bcp.2018.04.018.

[20] G. Wietzorrek, M. Drexel, M. Trieb, S.S. Sierra, Anti-inflammatory activity of small-molecule antagonists of Toll-like receptor 2 (TLR2) in mice, Imbio. 1 (2019) 1–9, https://doi.org/10.1016/j.imbio.2018.11.004.

[21] Z. Zhong, L. Liu, Z. Dong, L. Lu, M. Wang, C. Leung, D. Ma, Y. Wang, Structure-based discovery of an immunomodulatory inhibitor of TLR1-TLR2 heterodimerization from a natural product-like database, Chem. Comm. 51 (2015) 11178–11181, https://doi.org/10.1039/c5cc02728d.

[22] Q. Liang, Q. Wu, J. Jiang, J. Duan, C. Wang, M.D. Smith, H. Lu, Q. Wang, P. Nagarkatti, D. Fan, Characterization of Sparstolonin B, a Chinese Herb-derived Compound, as a Selective Toll-like Receptor Antagonist with Potent Anti-inflammatory Properties, J. Biol. Chem. 286 (2011) 26470–26479, https://doi.org/10.1074/jbc.M111.227934.

[23] S.K. Asrani, H. Devarbhavi, J. Eaton, P.S. Kamath, Burden of liver diseases in the world, J. Hepatology. 70 (2019) 151–171, https://doi.org/10.1016/j.jhep.2018.09.014.

[24] A. Bishayee, The role of inflammation and liver cancer, Adv. Exp. Med. Biol. 816 (2014) 401–435, https://doi.org/10.1007/978-3-0348-0837-8_16.

[25] M. Zhou, X. Zhu, S. Ye, B. Zhou, Blocking TLR2 in vivo attenuates experimental hepatitis induced by concanavalin A in mice, Int. Immunopharmacol. 21 (2014) 241–246, https://doi.org/10.1016/j.intimp.2014.04.027.

[26] J. Xu, X. Zhang, M. Monestier, N.L. Esmon, C.T. Esmon, Extracellular Histones Are Mediators of Death through TLR2 and TLR4 in Mouse Fatal Liver injury, J. Immunol. 187 (2011) 2626–2631, https://doi.org/10.4049/jimmunol.1003930.

[27] L. Wu, J. Sun, L. Liu, X. Du, Y. Liu, X. Yan, E.K. Osoro, F. Zhang, L. Feng, D. Liang, Y. Li, Q. Chen, S. Sun, L. Zhang, X. Lan, D. Li, S. Lu, Anti-toll-like receptor 2 antibody ameliorates hepatic injury, in ammation, brosis and steatosis in obesity-related metabolic disorder rats via regulating MAPK and NF-κB pathways, Int. Immunopharmacol. 82 (2020), 106368, https://doi.org/10.1016/j.intimp.2020.106368.

[28] Z. Papackova, M. Heczkova, H. Dankova, E. Sticova, A. Lodererova, L. Bartonova, M. Poruba, M. Cahova, Silymarin prevents acetaminophen-induced hepatotoxicity in mice, PLoS One. 13 (2018), e0191353, https://doi.org/10.1371/journal.pone.0191353.

[29] L. Liu, H. Li, K. Hu, Q. Xu, X. Wen, K. Cheng, C. Chen, H. Yuan, L. Dai, H. Sun, Synthesis and anti-inflammatory activity of saponin derivatives of δ-oleanolic acid, Eur. J. Med. Chem. 209 (2021) 112932, https://doi.org/10.1016/j.ejmech.2020.112932.

[30] B.G. de la Torre, F. Albericio, The Pharmaceutical Industry in 2019, An Analysis of FDA Drug Approvals from the Perspective of Molecules, Molecules 25 (2020) 745, https://doi.org/10.3390/molecules25030745.

[31] F. Peng, Q. Du, C. Peng, N. Wang, H. Tang, X. Xie, J. Shen, J. Chen, A. Review, The Pharmacology of Isoliquiritigenin, Phytother. Res. 29 (2015) 969–977, https://doi.org/10.1002/ptr.5348.

[32] K. Wang, Y. Yu, S. Hsia, Perspectives on the Role of Isoliquiritigenin in Cancer, Cancers 13 (2021) 115, https://doi.org/10.3390/cancers13010115.

[33] V.G. Yerra, A.K. Kalvala, A. Kumar, Isoliquiritigenin reduces oxidative damage and alleviates mitochondrial impairment by SIRT1 activation in experimental diabetic neuropathy, J. Nutr. Biochem. 47 (2017) 41–52, https://doi.org/10.1016/j.jnutbio.2017.05.001.

[34] D. Shi, J. Yang, Y. Jiang, L. Wen, Z. Wang, B. Yang, The antioxidant activity and neuroprotective mechanism of isoliquiritigenin, Free Radic. Biol. Med. 152 (2020) 207–215, https://doi.org/10.1016/j.freeradbiomed.

[35] Z. Song, Y. Zhang, H. Zhang, R.S. Rajendran, R. Wang, C. Hsiao, J. Li, Q. Xia, K. Liu, Isoliquiritigenin triggers developmental toxicity and oxidative stress-mediated apoptosis in zebrafish embryos/larvae via Nrf2-HO1/JNK-ERK/mitochondrion pathway, Chemosphere 246 (2020), 125727, https://doi.org/10.1016/j.chemosphere.2019.125727.

[36] X. Zhu, J. Liu, O. Chen, J. Xue, S. Huang, W. Zhu, Y. Wang, Neuroprotective and anti-inflammatory effects of isoliquiritigenin in kainic acid-induced epileptic rats via the TLR4/MYD88 signaling pathway, Inflammopharmacology 27 (2019) 1143–1153, https://doi.org/10.1007/s10787-019-00592-7.

[37] S. Anavi, O. Tirosh, iNOS as a metabolic enzyme under stress conditions, Free Radic. Biol. Med. 146 (2020) 16–35, https://doi.org/10.1016/j.freeradbiomed.2019.10.411.

[38] K. Ojiro, H. Ebinuma, N. Nakamoto, K. Wakabayashi, Y. Mikami, Y. Ono, C. Po-Sung, S. Usui, R. Umeda, H. Takaishi, Y. Yamagishi, H. Saito, T. Kanai, T. Hibi, MyD88-dependent pathway accelerates the liver damage of Concanavalin A-induced hepatitis, Biochem. Bioph. Res. Co. 399 (2010) 744–749, https://doi.org/10.1016/j.bbrc.2010.08.012.

[39] S.C. Funes, M. Rios, J. Escobar-Vera, A.M. Kalergis, Implications of macrophage polarization in autoimmunity, Immunology. 154 (2018) 186–195, https://doi.org/10.1111/imm.12910.